J. Fluid Mech. (2004), *vol.* 509, *pp.* 23–62.
DOI: 10.1017/S0022112004008778 Printed in the United Kingdom

The effect of two degrees of freedom on vortex-induced vibration at low mass and damping

By N. JAUVTIS AND C. H. K. WILLIAMSON

Sibley School of Mechanical and Aerospace Engineering, Upson Hall Cornell University
Ithaca, NY 14853, USA

(Received 2 May 2003 and in revised form 13 January 2004)

Although there are a great many papers dedicated to the problem of a cylinder vibrating transverse to a fluid flow (Y-motion), there are almost no papers on the more practical case of vortex-induced vibration in two degrees of freedom (X, Y motion) where the mass and natural frequencies are precisely the same in both X- and Y-directions. We have designed the present pendulum apparatus to achieve both of these criteria. Even down to the low mass ratios, where $m^* = 6$, it is remarkable that the freedom to oscillate in-line with the flow affects the transverse vibration surprisingly little. The same response branches, peak amplitudes, and vortex wake modes are found for both Y-only and X, Y motion. There is, however, a dramatic change in the fluid–structure interactions when mass ratios are reduced below $m^* = 6$. A new amplitude response branch with significant streamwise motion appears, in what we call the 'super-upper' branch, yielding massive amplitudes of 3 diameters peak-to-peak ($A_Y^* \sim 1.5$). We discover a corresponding periodic vortex wake mode, comprising a triplet of vortices being formed in each half-cycle, in what we define as a '2T' mode. We qualitatively interpret the principal vortex dynamics and vortex forces which yield a positive rate of energy transfer ($\dot{e}_V$) causing the body vibration, using the following simple equation:

$$\dot{e}_V = 2\Gamma^* U_V^* \dot{Y}$$

where Γ^* is vortex strength, U_V^* is the speed downstream of the dominant near-wake vorticity, and $\dot{Y}$ is the transverse velocity of the body. This simple approach suggests that the massive amplitude of vibration for the 2T mode is principally attributed to the energy transfer from the 'third' vortex of each triplet, which is not present in the lower-amplitude 2P mode. We also find two low-speed streamwise vibration modes, which is not unexpected, since they correspond to the first and second excitation modes of vibration for flexible cantilevers. By considering equations of motion for the two degrees of freedom, we find a critical mass, $m^*_{crit} = 0.52$, similar to recent Y-only studies, below which the large-amplitude vibrations persist to infinite flow velocity. We show that the critical mass m^*_{crit} is the same for the X- and Y-directions, which ensures that the shapes of X, Y trajectories can retain their form as the velocity becomes large. The extensive studies of vortex-induced vibration for Y-only body motions, built up over the last 35 years, remain of strong relevance to the case of two degrees of freedom, for $m^* > 6$. It is only for 'small' mass ratios, $m^* < 6$, that one observes a rather dramatic departure from previous results, which would suggest a possible modification to offshore design codes.

1. Introduction

There is a great deal of practical interest in the problems arising from vortex-induced vibration of structures, which occur in many branches of engineering, for example in aeroelastic applications where the fluid is air, yielding mass ratios (m^*) of order 100 (where $m^* =$ mass of oscillating structure/displaced fluid mass), or in hydroelastic applications in water, where m^* is of order 1 or 10. Most of the past research into such vibrations of cylindrical structures has been concerned with structures restricted to motions only transverse to a free stream, because the induced forces due to the vortex dynamics induce motions primarily in that direction. There have been only few studies of a fundamental nature which probe to what extent the allowance for an elastically mounted body to move in two degrees of freedom will modify the forces, responses and vorticity dynamics of the body in a flow. Of the experiments which study two degrees of freedom for an elastically mounted rigid cylinder, there appear to be no previous papers (to our knowledge) which study the most practical case, where both the mass and frequency are precisely the same in the two principal directions. However, in most practical cases, cylindrical structures (such as riser tubes or heat exchangers to name but two examples) have a mass ratio which is the same in both the streamwise (X) and transverse (Y) directions, and these structures have the same natural frequencies in these two directions. Contrasting with previous studies, we therefore focus on a design which ensures the same mass and the same frequencies in these two directions, and we introduce the resulting pendulum apparatus later in § 2.

Vortex-induced vibration of cylinders free to respond transverse to the fluid flow has been well studied, and several reviews discuss this problem (see for example Sarpkaya 1979; Bearman 1984; Williamson & Govardhan 2004). The work of Feng (1968) at high mass ratios, $m^* = 320$, demonstrates that the resonance of a body, when the oscillation frequency coincides with the vortex formation frequency, will occur over a regime of normalized velocity U^* (where $U^* = U/f_N D$, $U =$ free-stream velocity, $f_N =$ natural frequency; $D =$ diameter) such that $U^* \sim 5$ to 8. Two response amplitude branches are found, which are shown by Brika & Laneville (1993) and by Govardhan & Williamson (2000) to be due to two modes of vortex formation, as follows. For the 'initial' branch of response, the vortex wake comprises a '2S' mode, representing two single vortices formed per cycle. The 'lower' branch comprises the '2P' mode, whereby two vortex pairs are formed per cycle (as originally defined in Williamson & Roshko (1988) from their forced vibration study). However, at low mass and damping (m^* typically of the order 5–10), and higher amplitudes of response, three response branches are found to exist (Khalak & Williamson 1996, 1999; Govardhan & Williamson 2000), namely the initial branch (with a 2S vortex wake mode), the lower branch (with a 2P mode), and a further distinctly higher-amplitude mode appearing between these two other branches, namely the upper branch (also with a 2P mode of vortex formation). These modes and responses are found for strictly transverse vibration in a fluid flow. However, in a recent paper, which is a forerunner of the present contribution (Jauvtis & Williamson 2003), we have asked a key question, which remains significant in this work also:

To what extent are these transverse response modes and amplitudes influenced by the body's freedom to respond in the streamwise direction?

In our previous study, we were able to investigate this question for the particular case studied, namely the vibrations of an elastically mounted cylinder in a free stream,

although that preliminary study was limited to what we define as 'moderate' to large mass ratios, $m^* > 6$. Although this represents a light structure, compared with structures vibrating in air (with a mass, m^* of order 100) we shall subsequently find, in the present work, some dramatic differences in dynamics and flow phenomena, as one reduces the mass ratio of a vibrating body down to very small values of order 1 (in the regime we define as 'small' mass ratios). It is this very low-mass regime that we shall principally be concerned with in the present study, although it will be necessary to briefly present results for the moderate-mass structures, thus extending the work of Jauvtis & Williamson (2003).

At this point, we discuss two relevant studies, which have been carried out for systems enabling X, Y motion of an elastically mounted rigid cylinder, placed normal to a free stream. In the case of Moe & Wu (1990), the mass ratios in the X- and Y-directions are quite different (in one case, the mass oscillating in the Y-direction ($m^* = 7$) is double that in the X-direction), and also the natural frequencies are set in the ratio $f_X/f_Y = 2.18$. Under these chosen special conditions, they find a broad regime of velocity U^* over which resonant amplitudes are found (with normalized transverse amplitude close to $A^*_Y = A_Y/D = 1$), but no evidence of the different response branches, mentioned earlier for the Y-only motion studies. For Y motion, one expects a resonance when the speed of the flow is such that the vortex frequency for the non-oscillating body (f_V) is near to the structural natural frequency (f_N), which will occur when $U^* = U/f_N D \sim U/f_V D = 1/S$, where $S =$ Strouhal number. With a Strouhal number of around 0.2, one expects resonant oscillations near a velocity, $U^* \sim 5$. For their X, Y experiments, Moe & Wu find that the position of maximum response shifts to rather higher values of U^*, and reaches slightly higher amplitudes, compared with Y-motion experiments.

The subsequent experiments of Sarpkaya (1995) have concentrated on various ratios between f_X and f_Y, although he shows, within one plot, a set of amplitude data for X, Y motion where $f_X = f_Y$, indicating a 19% increase in amplitude and a shift to higher U^* for the peak transverse response, when compared with his Y motion case. In this case also, the oscillating masses in each of the X- and Y-directions are quite different (because, in the apparatus, one bearing system rides on top of another). Similar to the responses found by Moe & Wu (1990), he observed a response amplitude plot (A^*_Y versus U^*) showing a classical type of resonant response, with no evidence of distinct response branches.

In our present study, we shall find distinct response branches, or modes of response, as we shall show in §§3 and 4. In the present study, where both the mass and natural frequency are precisely the same in the X- and Y-directions, we shall see that there is indeed a marked similarity in the responses between X, Y and Y motion, but only down to mass ratios of around 6. For lower mass ratios, $m^* < 6$, a remarkable jump increase in amplitude response is found, corresponding to a new high-amplitude mode of response, which is quite distinct from the response phenomena in Y-only studies.

We show a schematic diagram in figure 1 of the two systems we are principally concerned with in this paper. A large body of literature exists concerning the case of motion restricted to only transverse motion (the Y-only case) in (a). In the case of X, Y motion in (b), we shall be concerned with a system which has precisely the same mass and natural frequency in the X- and Y-directions. In most cases, an excellent representation of the in-line $x(t)$ and transverse $y(t)$ displacements is given by the equations

$$x(t) = A_X \sin(2\omega t + \theta), \tag{1.1a}$$

$$y(t) = A_Y \sin(\omega t), \tag{1.1b}$$

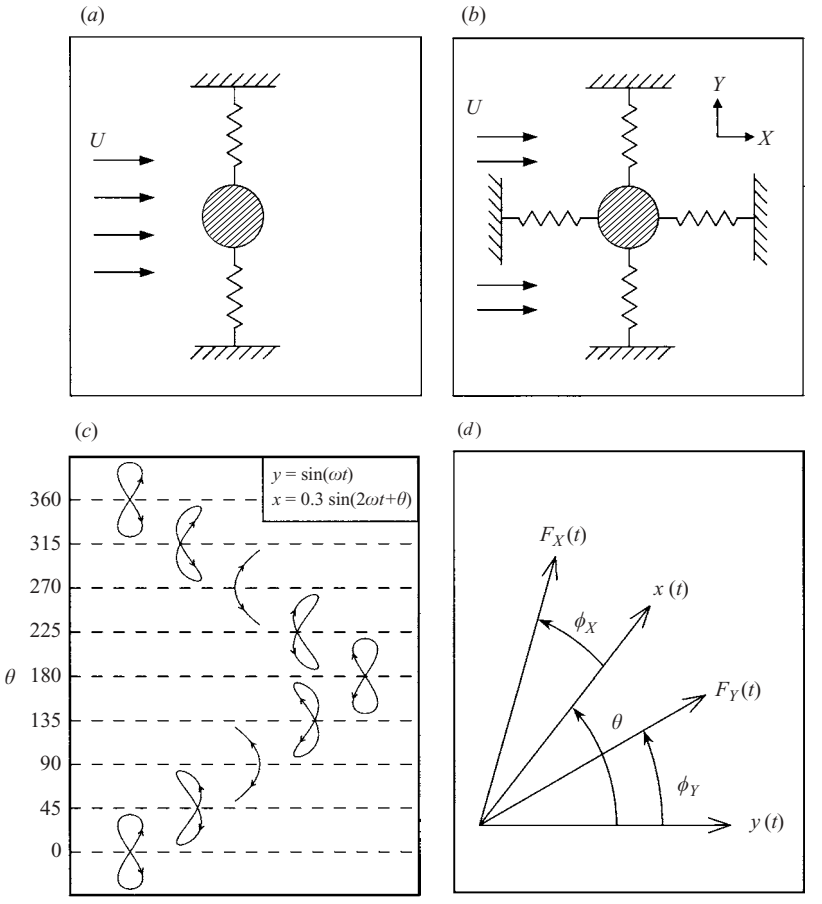

FIGURE 1. Definitions of the X, Y motion experiments. (a, b) Schematic diagrams of Y-only and X, Y motion experimental arrangements. (c) Typical X, Y trajectories, as a function of phase θ between X and Y motion (the free stream flows to the right). (d) Definition of the phase ϕ between force and displacement, for the X- and Y-directions.

and we exhibit these displacements (x and y), and their phase relationships (ϕ_X and ϕ_Y) to the forces (F_X and F_Y), in figure 1(d).

A different approach was adopted recently by Jeon & Gharib (2001), who forced a cylinder to move in the X- and Y-directions, in a fluid flow, under the prescribed motions given by equation (1.1). Specific phase angles, $\theta = 0°$ and $-45°$, were chosen, since they suggested that nature prefers a figure-eight type motion. For clarity, we present a useful schematic of the X, Y trajectory shapes for various values of phase angle between X and Y motion (θ) in figure 1(c). One of the most interesting results from the study of Jeon & Gharib appears to be the fact that even small amounts of streamwise motion ($A_X/A_Y = 20\%$) can inhibit the formation of the 2P mode of vortex formation. In fact, when they plot the actual cylinder trajectories through the fluid, it is difficult to tell the difference between the Y cases and the X, Y motions, yet the vortex dynamics can be distinctly affected. However, it should be mentioned that the free vibration studies of the present work, with a whole range of mass ratios chosen, indicate body motions which can be quite different from a figure-of-eight

motion as assumed above. In fact, at the highest amplitudes, the body trajectories are crescent-shaped (which is also the type of motion found for a tethered sphere in a flow, under resonant conditions: Govardhan & Williamson 1997, 2004), and the phase in this case has a value closer to $\theta = -90°$. Clearly, the choice of which amplitudes and phases are selected in a forced X, Y vibration experiment, out of a rather large set comprising combinations of four chosen parameters $\{A_X^*, A_Y^*, \theta, f_Y/f_X\}$, will influence the resulting conclusions.

It is significant to note that full-scale piles in an ocean current, and similar cantilever models in the laboratory, have been found to vibrate. Triggered by the structural failure of an offshore structure in the North Sea, Wooton *et al.* (1972) set up a full-scale cantilever (or pile) in the sea, and King (1974) subsequently conducted laboratory-scale experiments of a similar cantilever configuration. The measured vortex-induced vibrations involved significant streamwise motion, although the peak amplitudes of the cantilever tip ($A_X^* \sim 0.15$) are less than typically found for resonant transverse vibration of very light structures ($A_Y^* \sim 1.0$). As reviewed by Bearman (1984), and by Naudascher (1987), these streamwise vibrations are due to the fact that, as each vortex is shed (for the classical 2S mode), a fluctuating drag is generated, so that the in-line forcing frequency (f_X) is twice that for the transverse direction (f_Y). The forcing induces the body to vibrate in-line with the flow, if the normalized velocity is close to $U^* \sim \frac{1}{2}S$ (at which point, $f_X \sim f_N$), and King (1974) showed that the wake formation in this case comprised a classical vortex street (antisymmetric) pattern. Interestingly, these investigators also discovered a second mode of streamwise vibration, which occurred for slightly lower U^* (and slightly higher vibration frequencies for a given flow speed) when the wake formed symmetric vortex pairs close to the body, giving rise to a component of force in phase with the velocity, and an energy transfer from the fluid dynamics to the body motion.

One approach to understanding these two in-line vibration modes has been to conduct experiments where cylinders are forced to vibrate in-line with the free stream (without transverse motion). Griffin & Ramberg (1976) vibrated a cylinder at low Reynolds numbers ($Re = 190$) to find two different modes, one of which corresponds with the antisymmetric mode found for cantilevers. Ongoren & Rockwell (1988) found both cantilever modes of vortex formation, at the small amplitude of $A_X^* = 0.13$. They observed that, as the forcing frequency of the body (f) increased through $f/f_V = 1.8$, the mode of formation changed from a classical Kármán street type of wake to one where a vortex pair and a single vortex were formed per cycle (which may be defined as a 'P+S' mode in the terminology of Williamson & Roshko (1988) from their transverse forced experiments). As the forcing frequency in-line with the flow is further increased, Ongoren & Rockwell observed the symmetric vortex pair mode described earlier for cantilever studies. In the present work, there are some differences to these observations, as we shall see in § 3 and § 4, because the capability to vibrate transverse to the flow inhibits the asymmetric P+S mode, and one finds only modes which have a certain symmetry (the antisymmetric 2S mode, and the symmetric vortex pair mode). We shall find, in the present study, that an elastically mounted rigid cylinder in X, Y motion can also exhibit the two cantilever vortex formation modes discussed above, which is not an unexpected result.

Similar modes of in-line vibration have recently been reported, for an elastically mounted structure restricted to motion in-line with the flow, by Okajima *et al.* (2002), and for a model cantilever by Sugimoto *et al.* (2002). A further interesting experimental study by the group of Franz Hover and Michael Triantafyllou, employing the MIT

towing tank (Davis *et al.* 2000), has investigated the dynamics of a flexible cable, pin-jointed at each end, and towed through the fluid. The structure oscillates in the principal mode, with a maximum amplitude at central span, and it is of particular interest that the types of X, Y trajectories, as well as the response amplitude plot, exhibited by the cable, are qualitatively similar to those found in the present work for an elastically mounted (but rigid) body.

Numerical investigations have recently been conducted for elastically mounted cylinders in two degrees of freedom, typically at much lower Reynolds number (Re) than those studied experimentally. Blackburn & Karniadakis (1993), employing two-dimensional simulations at $Re = 200$, studied cases where they forced the body to vibrate, and also cases where they allowed free vibration in X, Y motion. In this laminar vortex shedding regime, they find smaller amplitudes (peak $A^*_Y = 0.6$) than are found in typical experiments at $Re \sim 10\,000$ (A^*_Y up to 1.0 typically) even when they set the damping to zero, which would give the limiting peak response attainable. Typical X, Y trajectories, for the low mass ratio of $m^* = 1.27$, had a figure-of-eight shape. For the specific cases studied, there does not appear to be much influence on the forces if one allows the body to move in two degrees of freedom, compared to Y-only motion. Newman & Karniadakis (1995) later provided some similar results to the Blackburn & Karniadakis work, but they also noted that there are differences in the vortex dynamics downstream between Y-only and X, Y-motion, if one forces the body with the same lateral frequency and amplitude of vibration in both cases. Subsequently, Newman & Karniadakis (1996) revealed, using three-dimensional numerical simulations at low Reynolds numbers ($Re < 300$), interesting travelling and standing wave patterns along flexible cables vibrating in a flow.

In the present study, we employ a pendulum system, which will ensure that our vertical cylinder apparatus has precisely the same mass and frequency in the X- and Y-directions. (It should be mentioned that an alternative approach is at present being adopted by the group of Donald Rockwell at Lehigh University, where they have designed an air bearing plate system, whose mass and frequency are also precisely the same in X- and Y-directions. Some close comparisons are being made between our systems, concerning early results of this study, in collaboration with Professor Rockwell.) Following a description of the experimental approach in § 2, we shall show, in § 3, that even down to mass ratios of $m^* = 6$, the freedom to move in two directions has very little effect on the responses and vortex dynamics modes, and these preliminary results have also been briefly presented in Jauvtis & Williamson (2002*a*, *b*, 2003). Further exploration in § 4 reveals the existence of a new and remarkably high-amplitude vibration mode, as one reduces the mass ratio to around $m^* = 4$. This response mode has a peak-to-peak amplitude of 3 diameters ($A^*_Y = 1.5$), and is caused by a new mode of vortex dynamics, that does not occur for strictly Y-only motion namely a '2T' mode, comprising a triplet of vortices that forms in each half-cycle of transverse body motion. Not only is the amplitude significantly larger than found hitherto for the 2P mode (typically $A^*_Y = 1$) but also the 2T mode will be shown, in § 4, to be more stable and periodic. We discuss the vortex dynamics (associated with the 2T mode) which give rise to the energy transfer from fluid to body motion that is required to sustain these high amplitudes. In § 5, we investigate the effect of mass ratio on the response dynamics, evaluating a similar value for the critical mass ($m^*_{crit} = 0.52$) to that which was found in Govardhan & Williamson (2000, 2002) for Y-only motion. Below this critical mass, the regime of velocities over which large-amplitude vibrations are found (ΔU^*) becomes infinitely wide. The use of equations of motion, and simple considerations, show that there is the same critical mass in the X- and Y-directions.

This is a reasonable result, when one considers the possibility for the shape of an X, Y trajectory to persist up to infinite normalized flow speed. We present the Conclusions in § 6.

2. Experimental details

We have constructed a hydroelastic apparatus, for particular application to very low mass and damping conditions, which operates in conjunction with the Cornell-ONR Water Channel. Refer to Khalak & Williamson (1996) for the details concerning this water channel facility, whose Lucite test section is 38.1 cm wide, with a water depth of 46 cm, and with a length of 250 cm. A horizontal plate is suspended over the water channel by four cables from the roof of the laboratory, and this plate acts as a pendulum, below which is mounted a vertical cylinder that reaches down into the fluid flow of the water channel. The cylinder is thus able to move in-line and transverse to the free stream, and has the same natural frequency (typically $f_N = 0.4$ Hz) and oscillating mass (m^* from 1.5 to 25.0) in these two directions, which was an essential design requirement. Cylinders of submerged length 38.1 cm, and diameter 3.81 cm or 5.08 cm, were used: in the same configuration as Khalak & Williamson. Very low values of the mass-damping parameters were used: $(m^* + C_A)\zeta = 0.001$ to 0.1 (where C_A is ideal added mass coefficient = 1.0, and ζ is the structural damping coefficient). Reynolds numbers ranged from 1000 to 15 000.

Where necessary, we were able to restrict the system to allow vibration only in the Y-direction, by the use of a pair of thin very long inextensible cables (5 m length) attached to the carriage, and extending to the wall of the laboratory far upstream. Under these conditions, it should be noted that there is excellent agreement, in the measurement of the body response, between the present pendulum arrangement and the set-up of Khalak & Williamson (1999), and also Govardhan & Williamson (2000), and some evidence for the agreement may be extracted from the plot of peak response given later in figure 4. Displacement was measured using magneto-strictive (non-contact) instrumentation. Digital particle image velocimetry (DPIV) was used to determine the vorticity in a horizontal plane midway down the submerged cylinder length, and the implementation of this technique is described in detail in Govardhan & Williamson (2000). In all presented colour contour plots of vorticity in this paper, the blue colour represents clockwise vorticity, while the red is for anticlockwise vorticity. In some cases, forces on the body are measured simultaneously with the measurement of displacements and vorticity field, and we describe the force measurement using linear variable displacement transducers in more detail in Khalak & Williamson (1996, 1997). The coordinate system is defined such that the origin is where the cylinder axis intersects the free surface; x is the downstream axis, y is the transverse axis, and z is the downwards vertical axis of the cylinder. The principal non-dimensional groups that we shall use in this study are laid out, for clarity, in table 1.

3. Response phenomena for moderate mass ratios ($m^* > 6$)

One of the principal interests in undertaking this research is to determine the extent to which the freedom to move in-line with the flow, simultaneously with the motion transverse to the flow, will modify the types of response that have been measured extensively in the literature for Y-only motions. We should point out that mass ratios around $m^* = 6$ are small by comparison with many of the previous studies of vortex-induced vibration, for example the classical experiments in air of Feng (1968), where

Mass ratio	m^*	$\dfrac{m}{\pi\rho D^2 L/4}$
Damping ratio	ζ	$\dfrac{c}{2\sqrt{k(m+m_A)}}$
Velocity ratio	U^*	$\dfrac{U}{f_N D}$
Amplitude ratios	A_Y^* A_X^*	$\dfrac{A_Y}{D}$ $\dfrac{A_X}{D}$
Frequency ratios	f_Y^* f_X^*	$\dfrac{f_Y}{f_N}$ $\dfrac{f_X}{f_N}$
Force coefficients	C_Y C_X	$\dfrac{F_Y}{\frac{1}{2}\rho U^2 DL}$ $\dfrac{F_X}{\frac{1}{2}\rho U^2 DL}$
Reynolds number	Re	$\dfrac{\rho U D}{\mu}$

TABLE 1. Non-dimensional groups. In this paper the added mass, m_A, is given by $m_A = C_A m_d$, where m_d is the displaced fluid mass and C_A is the potential added-mass coefficient. ($C_A = 1.0$ for a circular cylinder.) In the above groups, f_N = still-water natural frequency, D = cylinder diameter, L = cylinder length, ρ = fluid density, U = free-stream velocity, μ = viscosity.

he used mass ratios $m^* \sim 320$. However, in this study we wish to differentiate between the two regimes we investigate, as follows: where $m^* > 6$, we label this as 'moderate' mass ratios; where $m^* < 6$, we define this as 'small' mass ratios. In this section, we shall present the response dynamics, and the corresponding vortex dynamics, for the moderate mass ratios, where $m^* > 6$.

Previous studies, discussed earlier, would suggest that one might expect only minor changes in the maximum structural response when a system allows two degrees of freedom. This is supported by our measurements of the response for the case $m^* = 6.9$, and low mass-damping: $(m^* + C_A)\zeta = 0.0115$, shown in figure 2. Indeed, the response is surprisingly unaffected by the presence of two degrees of freedom. For comparison, we were able to restrain the X motion in one set of data, as mentioned in the previous section. The initial (I), upper (U) and lower (L) branches of response exist in the case of X, Y dynamics, as shown in figure 2, and there is good agreement with our data for Y-only motion. In one segment of the upper branch, the X, Y case rises to a level about 8% above the Y-only case, otherwise the agreement is closer. (Note also that we conducted extensive comparisons between our Y-only data, and the Y-only cases presented in Khalak & Williamson (1999) and in Govardhan & Williamson (2000), for various mass and damping combinations. The agreement is excellent, despite the radically different experimental arrangements.)

The modes of vortex formation for the X, Y motion are essentially the same as the modes found by Govardhan & Williamson (2000) for Y-only motion, where the initial branch is associated with the classical vortex street type of wake, defined as the 2S mode, seen in figure 3(a). The upper branch in (b) exhibits a 2P mode, although the second vortex of each pair is weaker than the first vortex. The lower branch also shows a 2P mode in (c), but with almost equal vortex strengths within each vortex pair. Further description of these modes can be found in Williamson & Roshko (1988) and in Govardhan & Williamson (2000). The essential point to note, at this stage of the study, is that the structural and the fluid dynamics are surprisingly unaffected

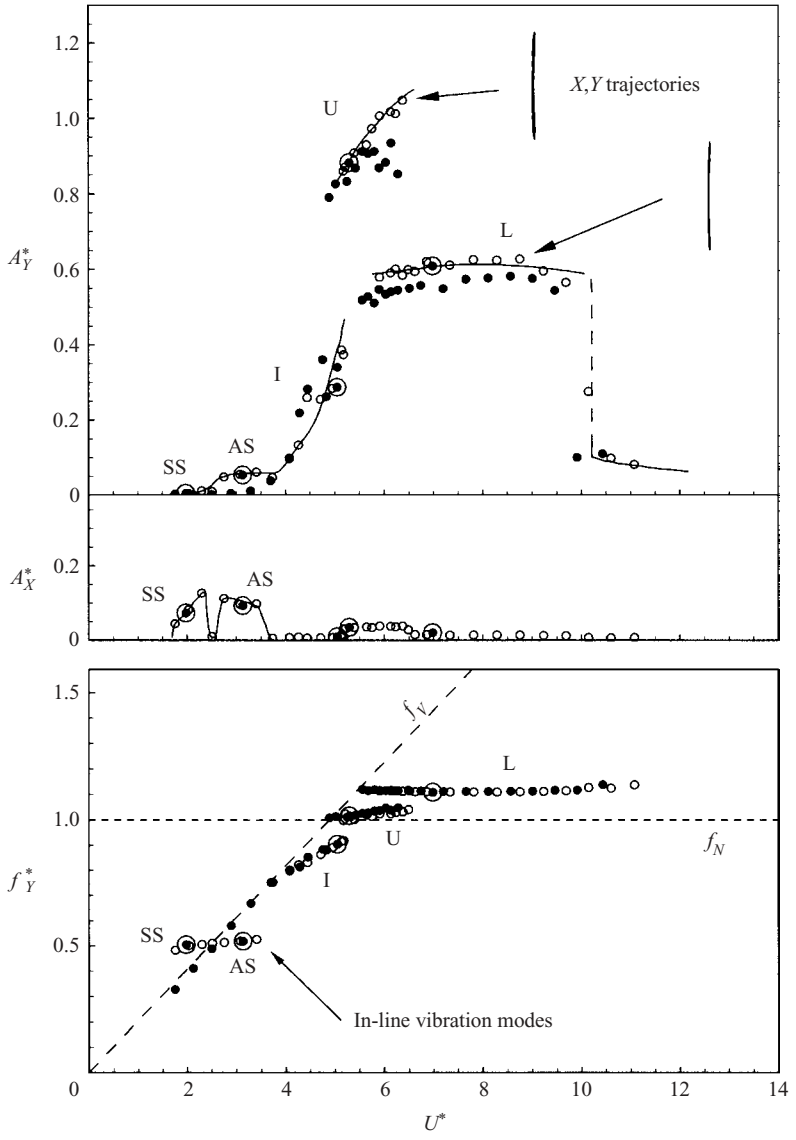

FIGURE 2. Response of the system for 'moderate' mass ratios ($m^* = 7.0$). Response amplitudes (A_X^* and A_Y^*) and transverse frequency (f_Y^*) are plotted as a function of normalized velocity (U^*). We compare the responses for the Y-only case (●), with the case for X, Y motion (○). Bull's eyes (⊙) refer to cases where we later present DPIV vorticity images. $Re = 2000$–$11\,000$. $(m^* + C_A)\zeta = 0.0117$.

by the freedom of the body to move streamwise as well as transverse to the flow, for moderate m^*. The X, Y trajectory shapes (in the upper plot of figure 2) show the lack of significant streamwise motion, exhibiting an almost flat crescent shape, for example, at the peak amplitude in the upper branch. The streamwise amplitudes in the plot of A_X^* are also small. It is therefore not unexpected that the transverse response modes for X, Y motion, and the vortex wake modes, should be the same as for Y-only dynamics. It might be noted that the phase angle between the in-line and transverse

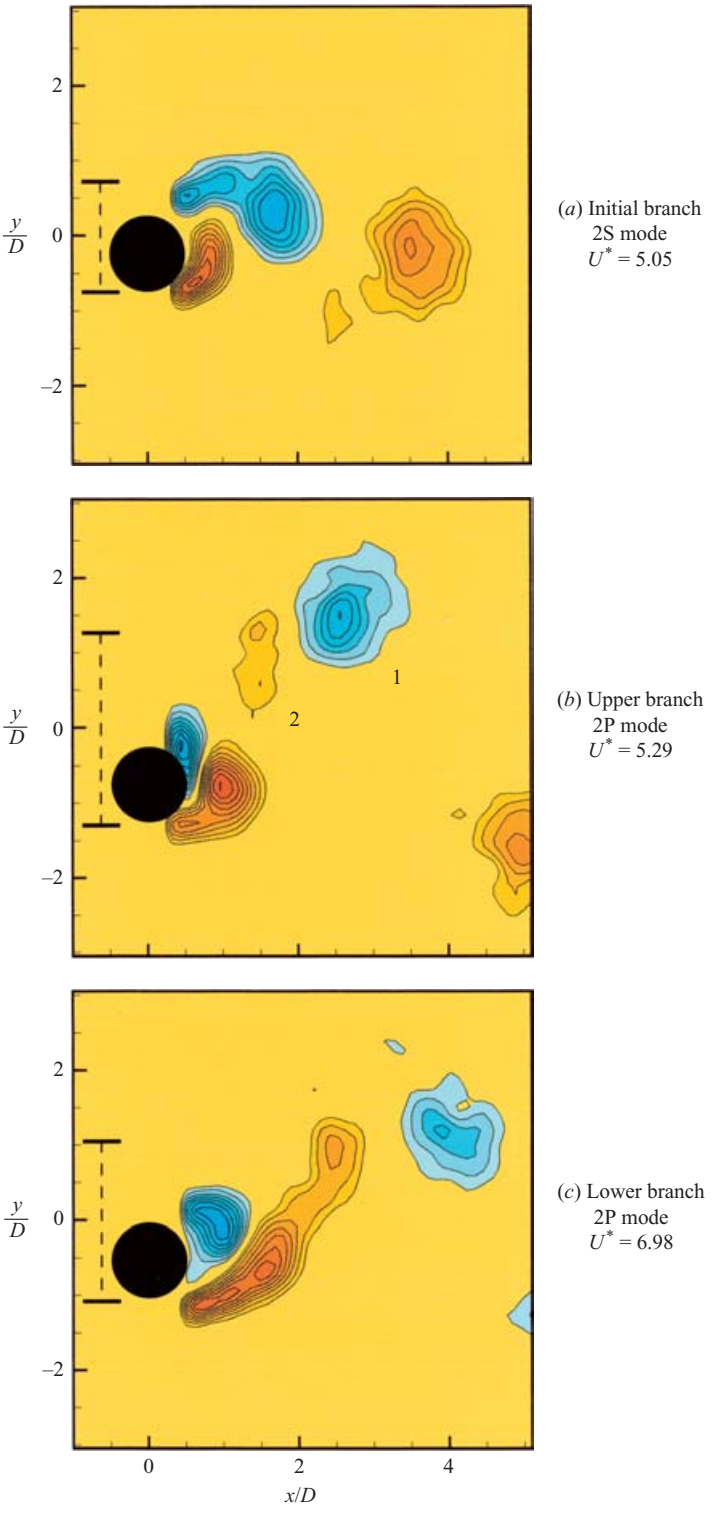

FIGURE 3. Vortex wake modes for 'moderate' mass ratios ($m^* = 7.0$) corresponding to the different response amplitude branches. In all cases, the cylinder is at the bottom extreme of its trajectory. Vorticity contour levels are $\{\omega D/U = \pm 0.5, \pm 1.0, \pm 1.5, \ldots\}$.

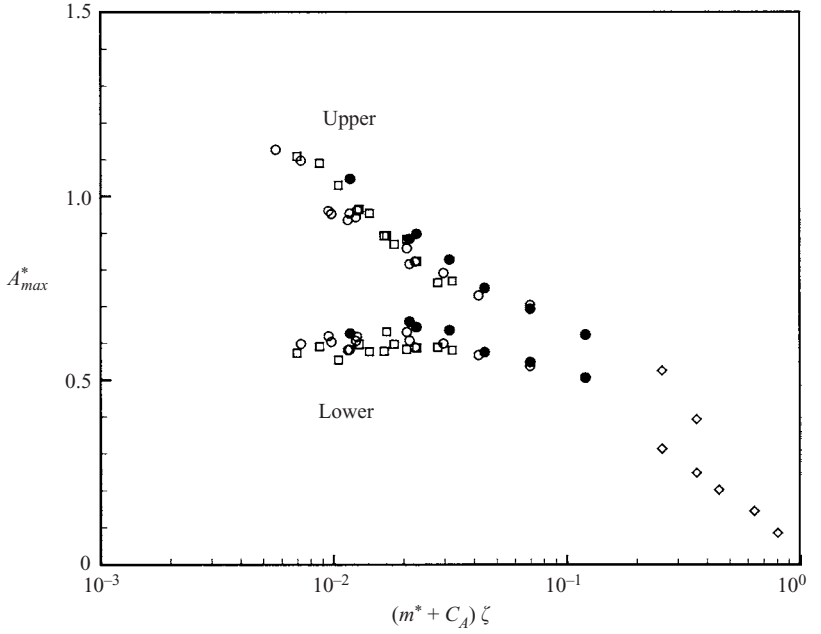

FIGURE 4. The 'Griffin' plot, for 'moderate' mass ratios ($m^* = 6$–25). This plot shows the variation of peak transverse amplitude (A^*_{MAX}) versus the mass-damping parameter ($(m^*+C_A)\zeta$). We compare X, Y motion (●), with the results for Y-only motion (○, present study; □, Khalak & Williamson (1999); ◇, Feng (1968)). Our X, Y data are for $Re = 1000$–12000.

motion (θ) is typically $\theta = 230^\circ$ to 270° (or -130° to -90°), within the upper branch regime.

Streamwise vibration modes are nevertheless observed if one moves to a regime of lower velocities, $U^* \sim 2.5$, as seen in figure 2, and one might expect to find these modes, based on the discussion of in-line dynamics in the Introduction. Because of the symmetry of the wake flow, we shall find, throughout this study, that the vortex dynamics induce a forcing frequency on the body in the streamwise direction (f_X) which is twice that induced in the transverse direction (f_Y): $f_X = 2f_Y$. We thus might expect a streamwise resonance, when $f_X \sim f_N$, or when $f^*_Y = f_Y/f_N \sim 1/2$, which corresponds in figure 2 with the branches denoted SS and AS. This regime of U^* is centred around $U^* = U/f_N D \sim 1/2S$, since $f_Y = f_V$, which is why the streamwise vibration is centred around $U^* \sim 2.5$. These modes SS and AS are defined in more detail in § 4, along with vorticity measurements, as they are more clearly observed at lower mass ratios.

A set of peak transverse amplitudes A^*_{max}, as a function of the mass-damping parameter $(m^* + C_A)\zeta$ have been plotted in the 'Griffin' plot of figure 4 (so-called after Griffin's original plots, similar to the one presented here; Griffin *et al.* 1975; Griffin 1980). There is only a slight difference between the peak responses measured for the X, Y motion and the Y-only case, across the complete data set, where $(m^* + C_A)\zeta = 0.01$–0.1, and where mass ratios vary in the range, $m^* = 6.0$–25.0. In summary, we see that the freedom to move streamwise is having almost no effect on the body dynamics, the response branches, and the wake vorticity dynamics. However, we shall now extend our study to lower mass ratios, in § 4, and we will discover a sharp departure from the scenario outlined above.

4. X, Y response modes for small mass ratios ($m^* < 6$)

In this section, we shall investigate the structural response at very low mass ratios, and a new high-amplitude branch will be discovered, which will be shown to correspond with a new mode of vortex formation. By studying also the induced forces on the body, we shall interpret what it is about the vortex formation that leads to the high amplitudes of vibration, employing a study of the rate of energy transfer during a cycle. We shall also briefly investigate the in-line vibration modes, which occur in a low-velocity regime.

4.1. *X, Y response*

If we reduce the mass ratio to $m^* = 2.6$, the first striking feature to appear in the amplitude response plot of figure 5 is the remarkably high amplitude of response, up to 3 diameters peak-to-peak, or $A_Y^* = 1.5$. As we conducted the experiment, it was somewhat surprising that, as the velocity was gradually increased, the amplitude kept increasing far beyond any value we had hitherto experienced in our Y-only experiments (where typical peak amplitudes are of the order $A_Y^* \sim 1$). We define this as the 'super-upper' branch of response, as distinct from the 'upper' branch of Y-only studies. What is also interesting is the in-line vibration amplitude, $A_X^* \sim 0.3$, which is significantly higher than the amplitudes of the in-line modes AS and SS, also shown in figure 5. We may also observe the other response branches in the plot, namely the initial branch (I), where the in-line vibrations are negligibly small, and the lower branch (L). The lower branch exhibits the same character as found for Y-only dynamics: a reasonably constant level of amplitude and frequency, from the start of the branch at $U^* \sim 8$ until this synchronization ends at $U^* \sim 12$. The small but discernible level of streamwise vibration ($A_X^* \sim 0.05$) is consistent with the fact that the lower-branch transverse amplitude level ($A_Y^* = 0.7$) is slightly above Y-only values ($A_Y^* = 0.6$). In conclusion, perhaps the most significant feature of the response measurements is the remarkably large transverse amplitude peak of $A_Y^* = 1.5$, which is far above previous measurements, and in excess of design codes generally employed to represent such vortex-induced vibration (Det Norske Veritas 2003).

Further features emerge from the measurements if one presents the response plots using a different normalized velocity. For given mass and damping, the response amplitude is a function of its oscillation frequency (f) relative to the frequency of vortex shedding in the absence of vibration (f_V). We therefore employ a normalized velocity $(U^*/f^*)S$, which is equal to (f_V/f), and which has previously yielded a good collapse of amplitude data for a set of response plots (made at different mass ratios), in Khalak & Williamson (1999) and in Govardhan & Williamson (2000). In the present case, using the plane $\{(U^*/f^*)S, A_Y^*\}$, we can also overlay the results onto the Williamson & Roshko (1988) map of vortex mode regimes found for Y-only forced vibration, shown in figure 6. Returning to our response data in figure 5, we initially felt that the initial and super-upper branches were all one branch. However, one might suggest that a break in the branch can be imposed at around $U^* = 5.0$, if one notes the change of slope of the A_Y^* curve, the sharply increasing streamwise motion, and the apparent but small change in the frequency curve (f_Y^*). However, the break between the initial and super-upper curves is much more evident in figure 6, with the modified velocity axis. It is quite interesting that the initial branch, with a 2S mode of vortex formation, terminates at the boundary of the 2S mode regime in the Williamson & Roshko map. At this point, there is a clear jump from the initial branch to what we define as the super-upper branch.

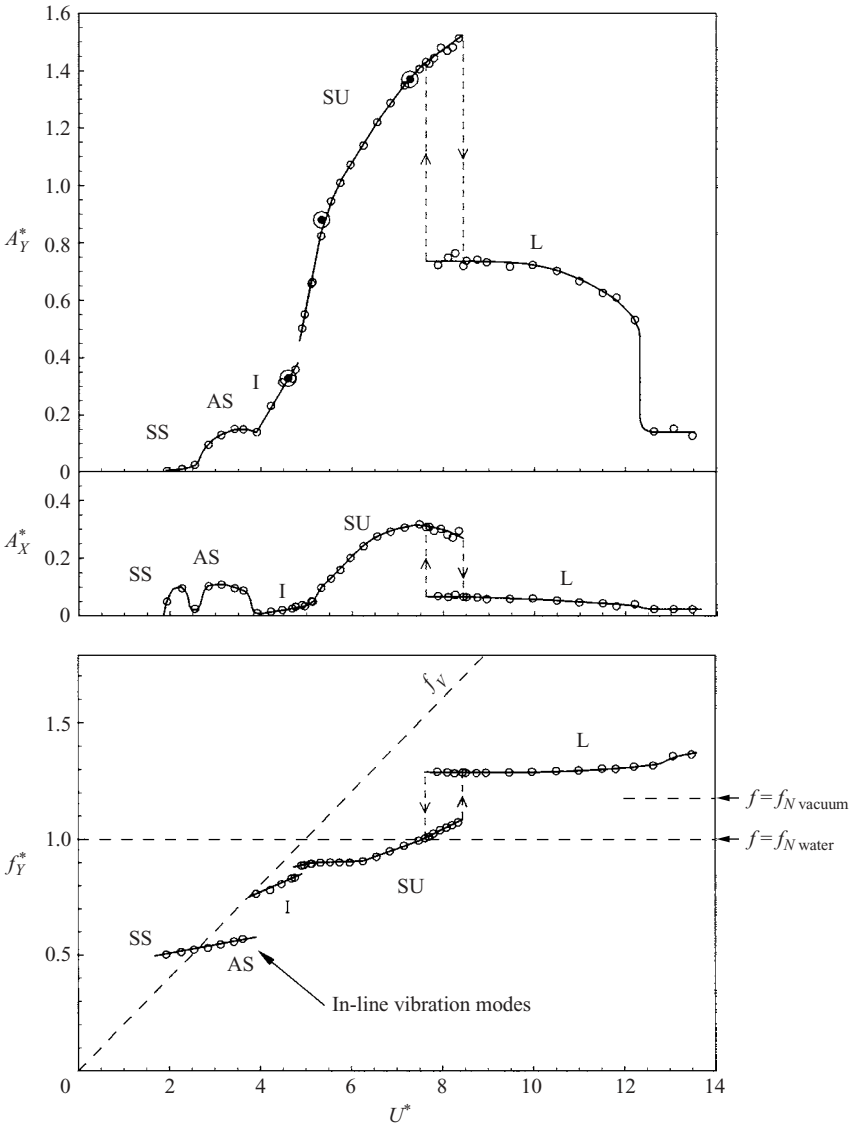

FIGURE 5. Response of the system for 'low' mass ratios ($m^* = 2.6$). Response amplitudes (A_X^* and A_Y^*) and transverse frequency (f_Y^*) are plotted versus normalized velocity (U^*). The overlap regime between the super-upper branch (SU) and the lower branch (L) exhibits a hysteresis, indicated by the arrows. In these plots, $(m^* + C_A)\zeta = 0.013$.

Although the super-upper branch will be shown later to correspond with a vortex mode different from the 2P mode, it is interesting that it starts at a (low-amplitude) 2P boundary, and also terminates at a (high-amplitude) 2P mode boundary in the Williamson–Roshko map (after which the vortex formation desynchronizes from the body motion in this map). The significance of the super-upper branch for X, Y vibrations terminating at the 2P boundary (relevant to Y-only motion), is not clear, and might represent a coincidence. Another surprising feature of such a presentation is the remarkably large region of overlap between the super-upper and lower branches,

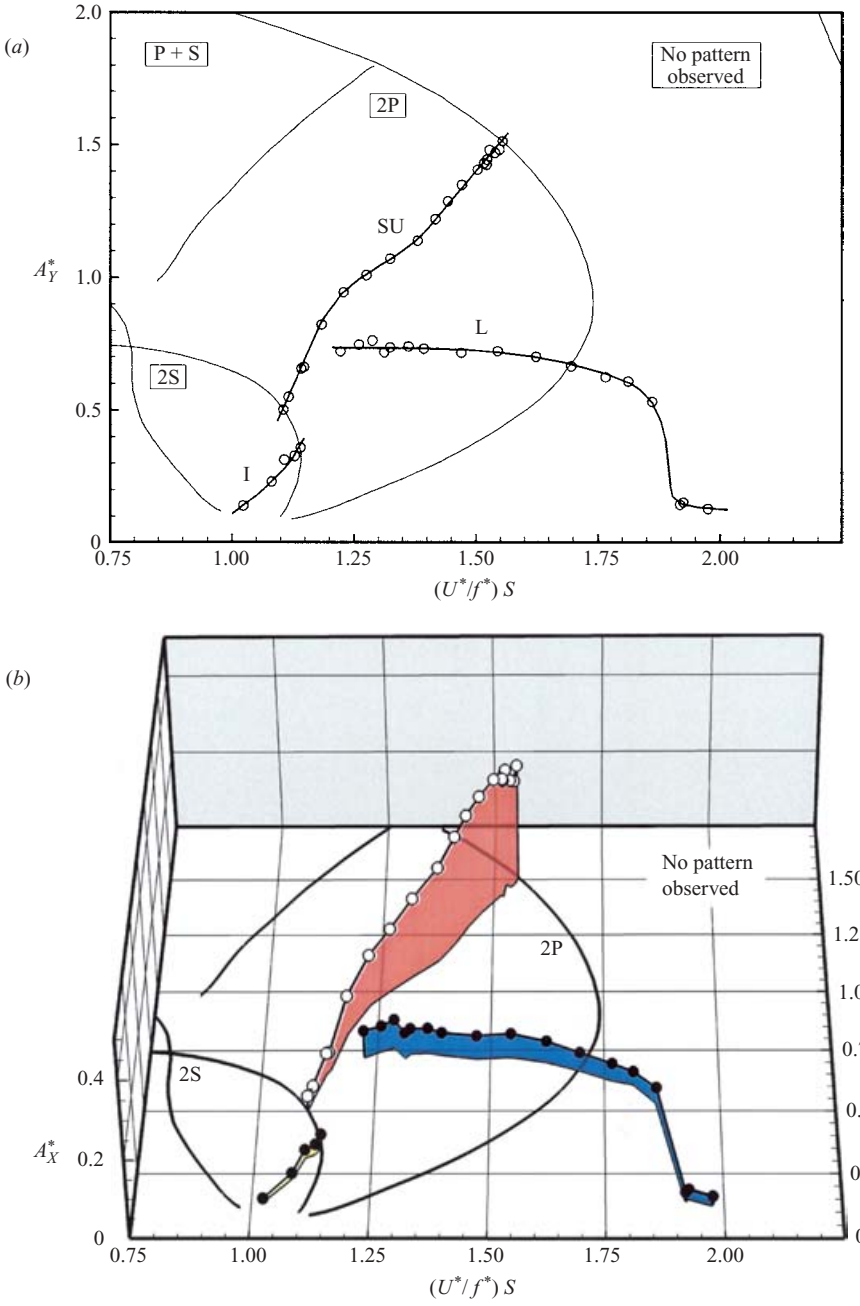

FIGURE 6. Response amplitude versus normalized velocity $(U^*/f^*)S$, for 'small' mass ratios ($m^* = 2.6$). (*b*) A three-dimensional response plot, where streamwise amplitude (A_X^*) is the vertical axis, and we superpose the Williamson & Roshko map of flow regimes in the horizontal plane where there is *Y*-only motion. The super-upper branch flies well above the map of regimes, yet interestingly starts and terminates above the 2P mode boundaries for Y-only motion. These plots also show clearly the distinction between the initial and super-upper branches.

extending over a range of velocities $(U^*/f^*)S = 1.2$–1.55. In this range, if one chooses a particular $(U^*/f^*)S$, the system can operate at either of two amplitude solutions, for the given mass and damping values.

We can generalize the response plot by including the streamwise amplitude (A_X^*) as a third axis in a three-dimensional plot, as shown in figure 6(*b*), where each response branch height is represented by a 'wall' of a specific colour. This is a useful presentation as it vividly exhibits the vibrations in the two principal directions. One can note that the horizontal plane represents the Y-only Williamson–Roshko map of regimes, and that other 'solution surfaces' might exist above this plane, in the case of X, Y motion, which would be chosen by the system, yielding net positive energy transfer from fluid to body motion. Our present super-upper branch represents just one possible line in such a surface. The phase angles between x and y motion (θ) on these solution surfaces would be those chosen by the freely vibrating system. One might conclude that attempting to explore such surfaces using forced vibration, with the huge choice of parameters, would be effectively very difficult. Analogous to our present figure 6 here, we use such a three-dimensional plot also in the case of the tip vibrations of a pivoted cylinder, in Flemming & Williamson (2004), and it is especially useful where a plot such as in (*a*) would otherwise allow two response branches to cross each other. In the latter study, we show that in fact such response branches are 'flying' at different heights above the horizontal plane. This also could be an explanation for the unusual result where two response branches cross each other in Brika & Laneville (1993). It is conceivable that such results reflect the presence of moderate streamwise motion as well as transverse motion.

Implementing the Hilbert Transform on the time traces of force and displacement, Khalak & Williamson (1999) were able to show that the transition between the upper and lower branches (for Y-only motion – see figure 2) involved an intermittent switching between these branches. In their case, the amplitudes of the two response branches were comparable, and the flow was able to switch between the upper-branch 2P vortex formation mode and the lower-branch 2P mode, although the mechanism of switching is not known (but could be related to three-dimensional effects, as suggested by Hover, Davis & Triantafyllou 2004, although such a scenario may be influenced by the experimental arrangement). An example time-trace of displacement $y(t)$ for Y-only motion close to the upper $\Leftrightarrow$ lower branch transition is shown in figure 7(*b*), and demonstrates the intermittent nature of the amplitude envelope, in marked contrast to the case for X, Y dynamics in the super-upper branch, shown in (*a*), where vibrations are remarkably periodic. In the present case, if the flow were to switch mode, it would have to do so between amplitudes of $A_Y^* = 1.5$ and 0.7, which is a jump in amplitude far larger than the jump associated with mode switching in Y-only motion. Instead of this scenario, we find that the super-upper $\Leftrightarrow$ lower transition is hysteretic. The hysteresis is represented in figure 5 by the vertical dashed lines. It is consistent with a hysteresis that the mode remains comfortably stable in the super-upper branch, and the displacement time trace $y(t)$ is remarkably stable and periodic, despite the very high amplitudes of the body vibration. This figure serves again to illustrate the massive amplitudes of the super-upper branch in comparison with the upper branch of Y-only motion.

In order to further characterize the system dynamics, we measure the phase angle θ between $x(t)$ and $y(t)$ motion, as defined in equation (1.1), in figure 8. The corresponding types of X, Y trajectory can be seen in idealized form in figure 1(*d*), and actual trajectories representing 100 cycles of motion are shown in the amplitude plot of figure 8, illustrating a striking periodicity in the body oscillations for all these cases. Of

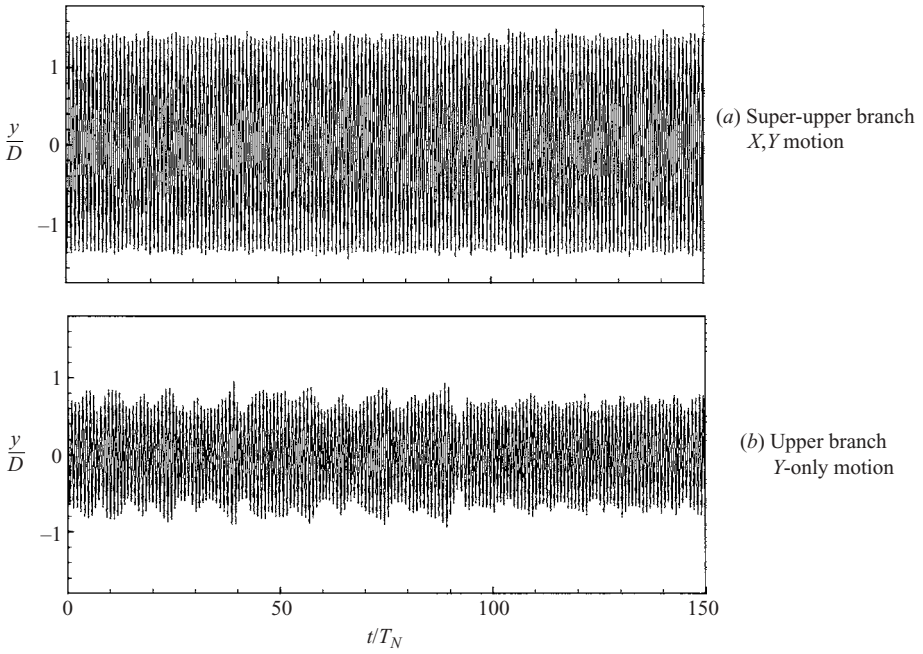

FIGURE 7. Time traces of displacement $y(t)$, showing in (a) the remarkable periodicity for the vibrations in the super-upper branch, despite the huge amplitudes. These oscillations are compared with the more intermittent vibrations of the upper branch of Y-only motion in (b). For both cases, $(m^* + C_A)\zeta = 0.013$. For (a), $U^* = 6.65$; for (b), $U^* = 8.35$.

course, the trajectories resemble usually a figure-of-eight type of motion, except when they are close to a phase angle of -90° or 270°, which is probably why investigators often quote the figure-of-eight shapes for these types of vibration problems, despite the fact that the phase θ can vary significantly. However, a characteristic shape at the limiting high amplitude of the super-upper branch is the crescent trajectory, where $\theta = 270^\circ$, and is similar to what is seen for tethered or elastically mounted spheres (Govardhan & Williamson 2004), and for pivoted cylinders (Flemming & Williamson 2004).

One might now ask the question of how such a super-upper branch alters the character of the 'Griffin' plot (of figure 4), where peak transverse amplitudes (A^*_{MAX}), are plotted as a function of mass-damping $(m^* + C_A)\zeta$. We have plotted such peak amplitudes in figure 9, for small mass ratios ($m^* = 2.5$–3.2), and for a variety of Reynolds numbers ($Re = 3300-15\,300$), showing the peak amplitude levels of both the super-upper branch and the lower branch. It is clear that the super-upper amplitudes are far in excess of the kinds of amplitudes commonly used in such data plots in design practice, such as in Det Norske Veritas (2003) design codes in offshore design, which are based on the much-studied Y-only experiments. It is also worth noting that the levels of the super-upper and lower branch peak responses are apparently independent of Reynolds number within the range investigated here.

As one gradually reduces the mass ratio m^*, in figure 10, at a fixed mass-damping (in this case $(m^* + C_A)\zeta = 0.013$), the peak amplitude A^*_Y is not affected, and remains at the value of the upper branch, until one reaches $m^* = 6$. At this point the streamwise amplitude (A^*_X) starts to increase, as m^* is further reduced, although

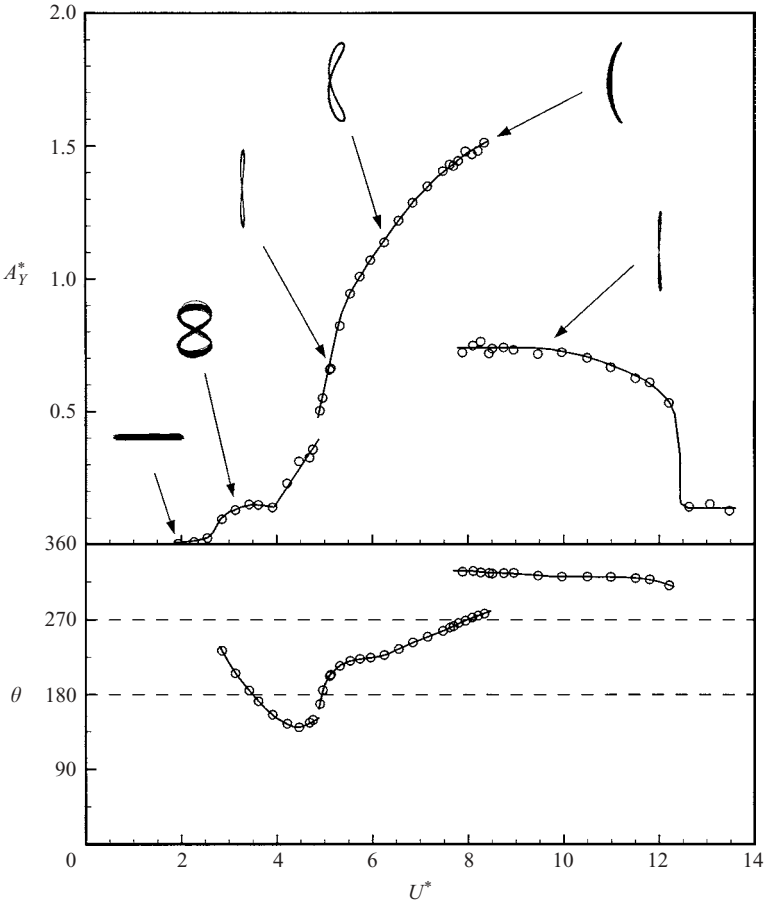

FIGURE 8. X, Y trajectory shapes (Lissajous figures), and corresponding phase angles between X and Y motion. (The shapes are not to scale with each other.) The response in this case is for $m^* = 2.6$, $(m^* + C_A)\zeta = 0.013$.

the amplitude envelope itself becomes unsteady or transient. It is only when the amplitude reaches the super-upper branch, for a mass ratio $m^* = 4$ that the vibrations reach a stable periodic solution (for which we have the example in figure 7*a*). The relative magnitude of streamwise to transverse amplitudes in the super-upper branch appears to saturate at a level of 20% as the structure becomes very light.

4.2. *Discovery of a '2T' vortex formation mode*

The appearance of a new type of response branch, for sufficiently low-mass structures in X, Y vibration, would suggest that there is a corresponding vortex formation mode, quite distinct from the known modes in vortex-induced vibration. This is indeed the case, as shown in figure 11, where we find a new mode of vortex formation comprising three vortices being formed per half-cycle of body motion. We define this the '2T' mode, comprising two *triplets* of vortices per cycle (in accordance with the terminology introduced in Williamson & Roshko 1988). In this mode, we may observe vortices 1 and 2 in figure 11(*a*), comprising a counter-rotating vortex pair, which can be compared directly to the vortex pair of the 2P mode in figure 3(*b*), also marked as vortices 1 and 2, at the same phase of the cyclic body motion. The major difference

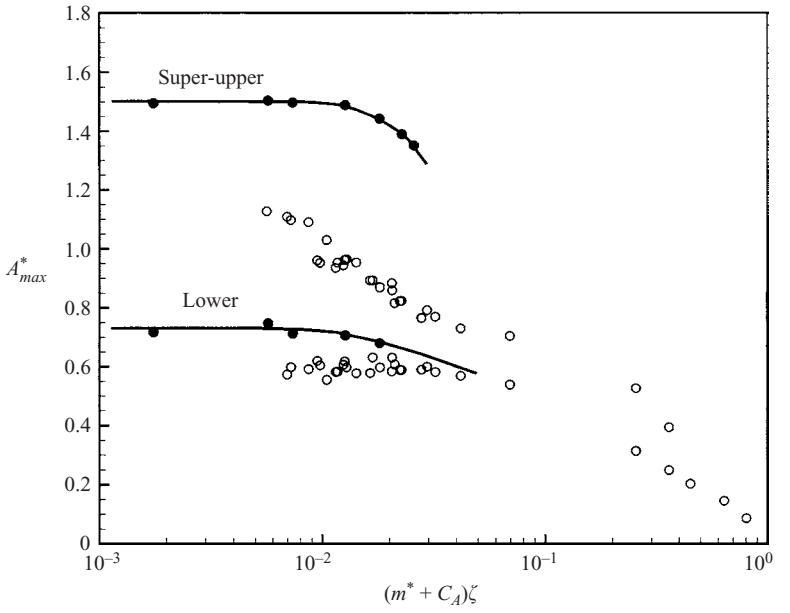

FIGURE 9. The 'Griffin' plot, for 'small' mass ratios ($m^* = 2.5 - 4.0$). This plot shows the variation of peak transverse amplitude (A^*_{MAX}) versus the mass-damping parameter ($(m^* + C_A)\zeta$). The data for X, Y motion (●) in the super-upper branch are for Reynolds numbers (from leftmost point, moving right): 5900, 15300, 11600, 6100, 6700, 3300, 4600, and $m^* < 5$. The data for Y-only motion (○) are as in figure 4.

at this point in the cycle, for the 2T mode, appears to be the third principal vortex (labelled 3) which is generated in addition to the classical vortex pair. We make this clear in figure 12(a, b), where we have encircled the vortex pair P in both the 2T and 2P modes, at the same phase within the cycle. This vortex pair P comprises one half of the 2P vortex wake mode. Thus, we can see that the essential difference between the modes is the extra vortex 3, which we might expect is responsible for the markedly different system dynamics, as we shall study later.

If we focus now on figure 11(d, e, f), it seems that it is the significant acceleration of the body at the top of the cycle that generates a fresh pair of vortices (vortices 2 and 3), which are placed in proximity to the strongest vortex 1. (Such a vortex 1 appears to form in all of the observed vortex modes, namely the 2T, 2P and 2S modes.) An illustration of this 'starting' vortex pair (vortices 3 and 2), due to the strong acceleration, is particularly evident in frame (f), and is also shown, for clarity, in figure 12(c), where other vorticity has been removed from the image. We label this 'starting' vortex pair, generated at the start of the acceleration phase, as P_S in (c), to distinguish it from the vortex pair P discussed earlier in (a) and (b). We might note also that although vortices P_S appear to represent starting vortices, their strengths are nevertheless different, and the clockwise blue vortex 3 is somewhat stronger than its partner red vortex, as evident from figure 11.

4.3. *Forces for X, Y modes*

We have been able to measure the forces on the body during its free vibration, simultaneously with the measurement of displacements, and in some cases also during the measurement of the wake vorticity field. In the case of the initial and lower

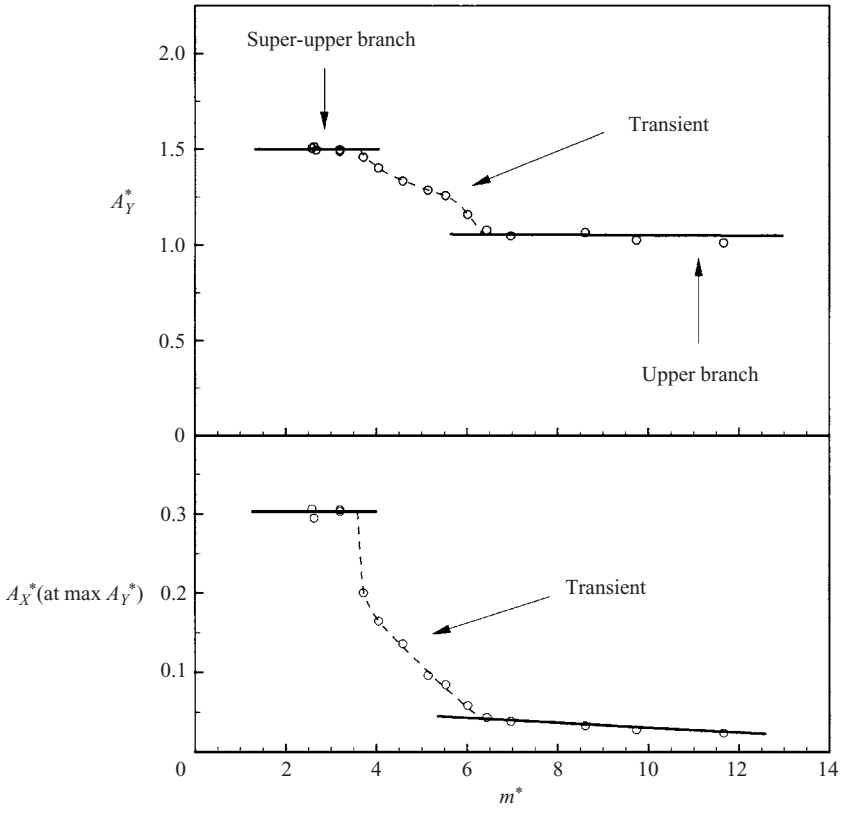

FIGURE 10. Variation of peak amplitudes (A_X^* and A_Y^*) as a function of mass ratio (m^*). Above $m^* = 6$, the response is similar to the case of Y-only motion. Below $m^* = 6$, there is a departure from Y-only response, which exhibits an unsteady amplitude envelope behaviour (labelled 'transient'), between $m^* = 4.0$ and 6.0. Below $m^* = 4.0$, there is a remarkable periodicity in the amplitude response, which persists to lower m^*. For these data, $Re \sim 6000$, $(m^* + C_A)\zeta \sim 0.013$.

branches, the forces are quite similar to the measurements described in Khalak & Williamson (1997, 1999) and in Govardhan & Williamson (2000). Therefore, in the present work, we shall focus on the super-upper branch, in figure 13. As the amplitude increases (down the figure), the force profiles $C_Y(t)$ that oscillate principally at the fundamental frequency (f), develop also a superposed distinct $3f$-component, which we will later associate with the principal vortex dynamics of the 2T mode. Despite the fact that the forcing is quite non-sinusoidal, the displacement remains remarkably close to sinusoidal. Further analysis and an understanding of this point is put forward in Williamson & Jauvtis (2004*a*, *b*) who show that the transfer function between force and displacement effectively filters out the $3f$-component and higher harmonics in the force. The development of the $3f$-component in the force is illustrated well by the (Y, C_Y) phase plots in the third column of figure 13.

The phase plots of (C_Y, C_X) in figure 14 exhibit intricate shapes. As the normalized velocity U^* is increased, and thereby also the transverse amplitude is increased, these plots are indicative of the development of the $3f$-component in the transverse force (vertical) direction, and the $2f$-component in the streamwise (horizontal) direction. In the case of the streamwise force, C_X, this is of course the principal force and vibration frequency in that direction. It can be seen that large instantaneous total

https://doi.org/10.1017/S0022112004008778 Published online by Cambridge University Press

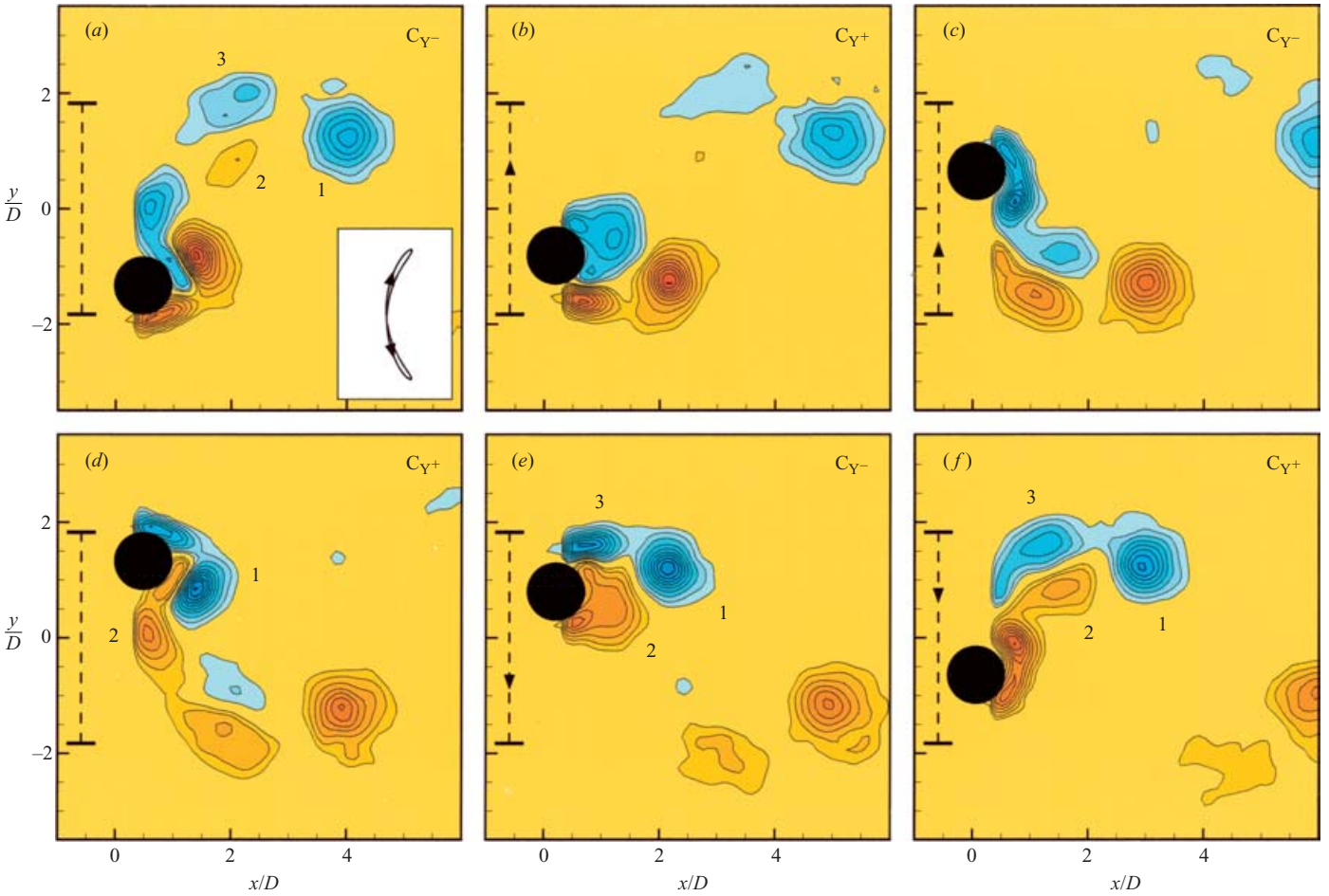

FIGURE 11. '2T' vortex wake mode.This new mode of vortex formation comprises a triplet of vortices forming in each half-cycle (see vortices 1-2-3 for example). In this case, $m^* = 2.6$; $Re = 5300$; $A_Y^* = 1.33$; $U^* = 7.27$. Vorticity contours are $\{\omega D/U = \pm 0.4, \pm 1.2, \pm 2.0, \ldots\}$.

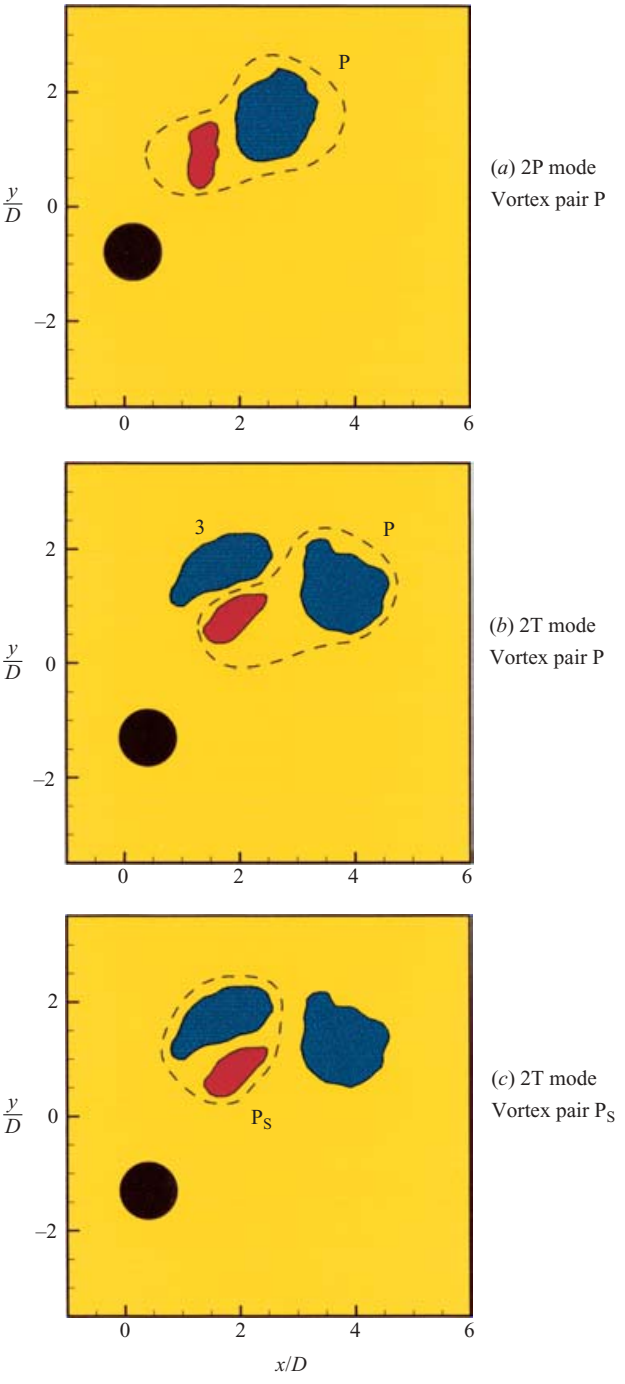

FIGURE 12. The '2T' and '2P' vortex wake modes. In (*a*) and (*b*), we note the marked similarity in the formation of the vortex pair, P, for both the 2T and 2P modes. (This pair P corresponds to one half of the 2P mode vortex formation). For the 2T mode there is a strong additional clockwise (blue) vortex 3 formed, above the vortex pair P. In (*c*), we show what we define as the 'starting vortex pair', P_S, created due to the intense acceleration just as the body plunges down from the top of its trajectory.

https://doi.org/10.1017/S0022112004008778 Published online by Cambridge University Press

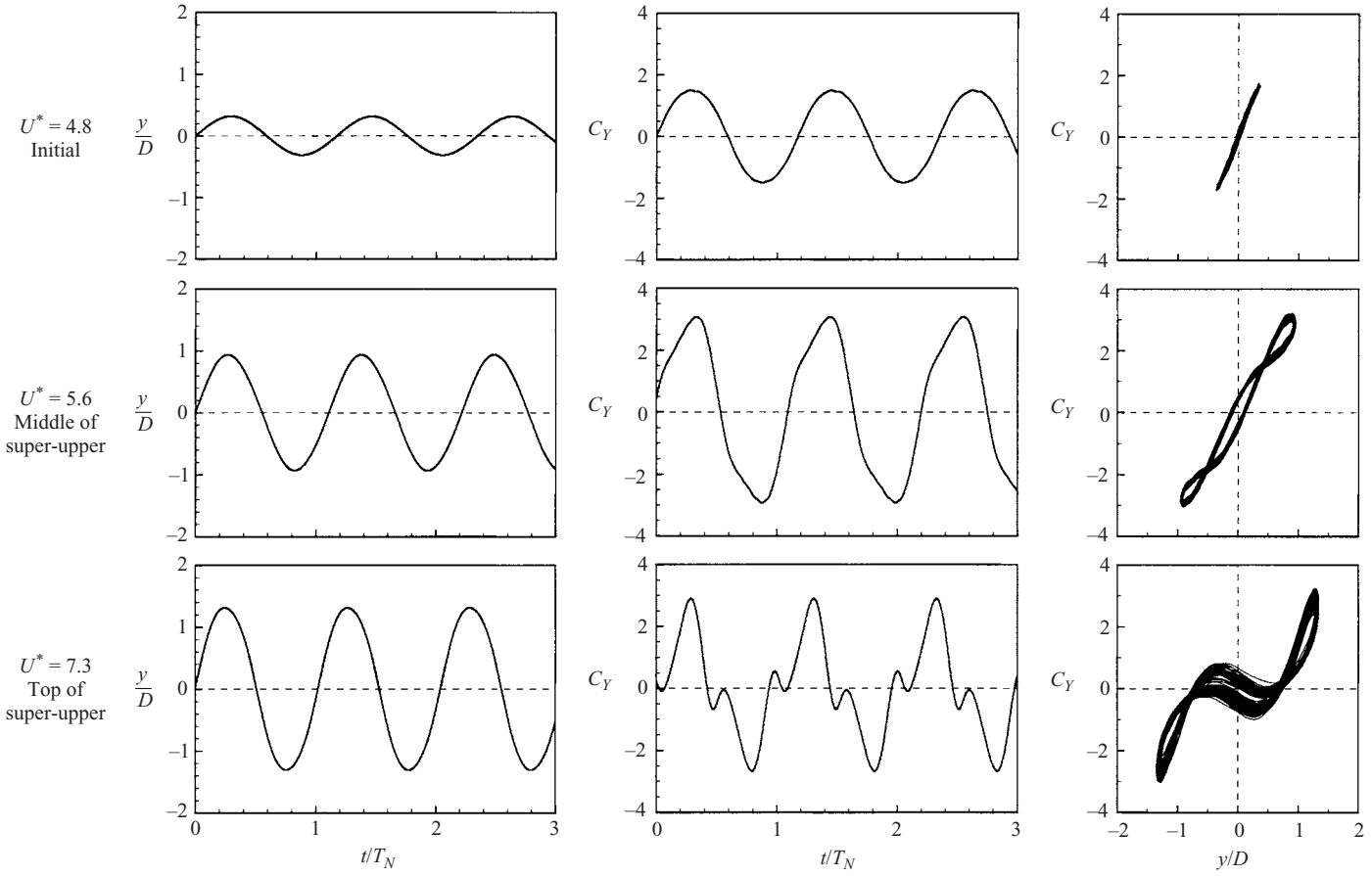

FIGURE 13. Displacement, $Y(t)$, and transverse force, $C_Y(t)$, profiles in the initial branch and the super-upper branch. We also exhibit phase plots of $\{Y, C_Y\}$. In this figure, $m^* = 2.6$; $(m^* + C_A)\zeta \sim 0.013$.

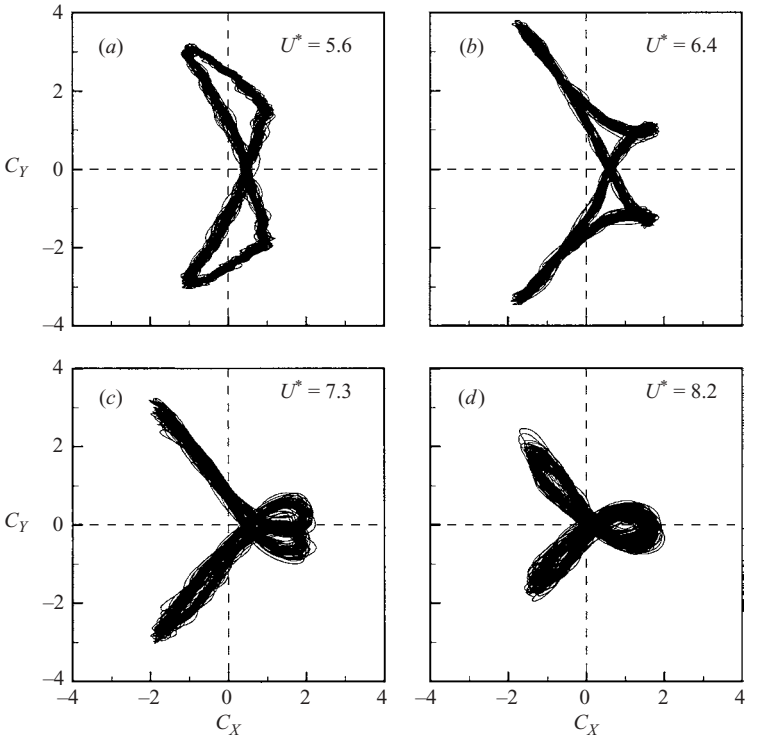

FIGURE 14. Phase plots of $\{C_X, C_Y\}$, on ascending the super-upper branch, with increasing velocity U^*. This figure also serves to illustrate the remarkable periodicity of the super-upper branch X, Y response, since we note that we show around 100 cycles of oscillation in each phase plot. In this figure, $m^* = 2.6$; $(m^* + C_A)\zeta \sim 0.013$.

force coefficients (vector sum of C_X and C_Y) in excess of 4.0 are developed. The final phase plot in (*d*) shows the limiting case at the very top of the super-upper branch, when the actual X, Y body trajectory through the fluid is the crescent shape of figure 8.

Measurements of force coefficients on a low-mass body ($m^* = 2.6$), able to execute X, Y motion, are presented in figure 15, and correspond to the amplitudes and frequency plots of figure 5. The forces in this case may be compared with those measured for a comparable mass ratio, $m^* = 3.3$ in Khalak & Williamson (1999), applicable to Y-only motion. There is at least a 6-fold increase in the fluctuating lift force (peak $C_{Yrms} = 2.1$), and around a 5-fold increase in the maximum drag force felt during a cycle (peak $C_{Xmax} = 5.1$), with a mean drag force of $C_{Xmean} = 3.0$, compared to data for a non-oscillating body. Although there is thus a large increase in forces due to the vibration, the increase is interestingly not as dramatic as would be assumed if one extrapolated from the data for Y-only motion. The plots in figure 15 also show the phases ϕ_Y and ϕ_X, as defined in figure 1(*d*), based on the f-component of the force $C_Y(t)$. There is a jump in phase ϕ_Y as one transitions from the super-upper to the lower branch, and this corresponds with the fact that the frequency of vibration (f) passes through the natural frequency of the system in vacuo, as indicated in the frequency (f^*) plot in figure 5. (Further discussions of this type of phase jump are found in Khalak & Williamson (1997, 1999). The relationship of such jumps to the

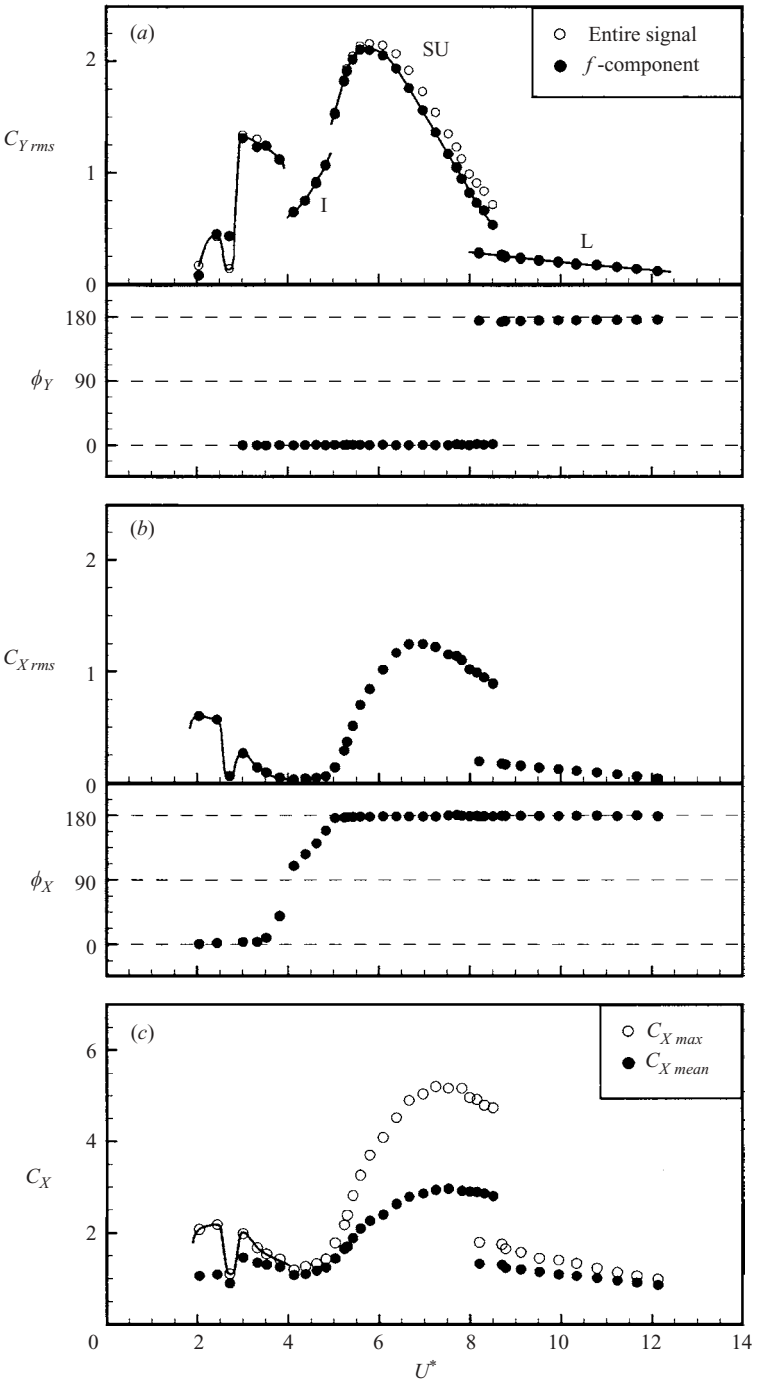

FIGURE 15. Force coefficients and phase angles through the synchronization regime. In this figure, $m^* = 2.6$; $(m^* + C_A)\zeta \sim 0.013$.

frequency (f^*) in water and in vacuo, are found in Govardhan & Williamson (2000), where they introduce a second equation of motion involving vortex force and 'vortex phase' to explain these jump phenomena.)

4.4. *Vortex dynamics and energy transfer*

At this point, we wish to understand just what it is about the vortex dynamics that enables the body to vibrate at such high amplitudes in the super-upper branch, during the presence of the 2T mode. The displacement is close to sinusoidal, with only a small $3f$-component, although the force, especially the force associated solely with the vortex dynamics, can have a distinctly non-sinusoidal profile. In order to make the link between this and energy transfer, we shall show that the energy transfer from fluid to body motion over a cycle is the product of the transverse vortex force (F_V) times the transverse velocity ($\dot{y}$), integrated over one cycle of motion. (This is distinct from the classical approach, which would be to find the energy transfer employing the total force.) Under steady state conditions, the energy transfer over a cycle must be positive for the motion to exist, and is equal to the energy dissipated into the structural damping (and will thus be a very small value in these low-damping experiments).

As performed in Govardhan & Williamson (2000), and based on the suggestions of Lighthill (1986) (and private communication, 1979), we shall decompose the total force into a potential added mass force (F_P) and a vortex force component (F_V) that is due to the dynamics of what is called the 'additional vorticity'. ('Additional vorticity' refers to the entire vorticity in the flow field, minus that 'part of the distribution of vorticity attached to the boundary in the form of a vortex sheet allowing exactly the tangential velocity (slip) associated with the potential flow', as stated by Lighthill.) A full knowledge of the vorticity field would yield the vortex force through the concept of vorticity impulse:

$$F_V = \frac{1}{2}\rho \frac{\mathrm{d}}{\mathrm{d}t} \int (\boldsymbol{\omega}_A \times \boldsymbol{x})\, \mathrm{d}V \tag{4.1}$$

where ω_A is the additional vorticity within a volume V, and x is the position of the vorticity. The vortex force is related in a definite way to vortex dynamics and to the convection of vorticity. The total transverse force (F_Y) is given as

$$F_Y(t) = F_P(t) + F_V(t). \tag{4.2}$$

Normalizing all the forces by ($\frac{1}{2}\rho U^2 DL$) gives the simple relation

$$C_Y(t) = C_P(t) + C_V(t). \tag{4.3}$$

The instantaneous potential added mass force $F_P(t)$ acting on the body is given by

$$F_P(t) = -[C_A m_d\, \ddot{y}(t)] \tag{4.4}$$

where m_d is the displaced fluid mass: $m_d = (\pi\rho D^2 L/4)$. If we were to assume for the moment a sinusoidal response, $y = A_Y \sin(\omega t)$, then we could write the normalized potential force, $C_P(t)$ as

$$C_P(t) = 2\pi^3 \frac{(y(t)/D)}{(U^*/f^*)^2}. \tag{4.5}$$

However, in the following equations, we shall not in general make such an assumption of precisely sinusoidal force or response. The total energy transfer from fluid dynamics to body motion over a cycle (i.e. the work done by the fluid force) is given as

$$E = \int_0^T F_Y(t)\dot{y}(t)\, \mathrm{d}t \tag{4.6}$$

which becomes, using (4.2),

$$E = \int_0^T F_P(t)\dot{y}(t)\,\mathrm{d}t + \int_0^T F_V(t)\dot{y}(t)\,\mathrm{d}t, \tag{4.7}$$

$$E = E_P + E_V, \tag{4.8}$$

where E_P is the energy transfer associated with the potential force, and E_V is that due to vortex force. An expression for E_P may thus be given as

$$E_P = -\int_0^T [C_A m_d\,\ddot{y}(t)]\dot{y}(t)\,\mathrm{d}t. \tag{4.9}$$

We now consider the velocity $\dot{y}(t)$ to be a periodic function:

$$\dot{y}(t) = \sum A_n \cos(n\omega t + \phi_n) \tag{4.10}$$

so that the expression for E_P becomes

$$E_P = C_A m_d \int_0^T \left[\sum A_n \cos(n\omega t + \phi_n)\right]\left[\sum A_n n\omega \sin(n\omega t + \phi_n)\right]\,\mathrm{d}t. \tag{4.11}$$

After a lengthy but straightforward analysis, one finds that $E_P = 0$ for such periodic functions, so that the total energy transfer (E) is simply the energy transfer associated with the vortex force (E_V):

$$E = E_V = \int_0^T F_V(t)\dot{y}(t)\,\mathrm{d}t. \tag{4.12}$$

We can define here the normalized rate of energy transfer, due to the vortex dynamics, as

$$\dot{e}_V(\tau) = C_V(\tau)\dot{Y}(\tau) \tag{4.13}$$

where $\tau = t/T$, and $\dot{Y}(\tau) = \dot{y}/D$. The normalized energy transfer over a complete cycle (E_V^*) is thus

$$E_V^* = \int_0^1 \dot{e}_V(\tau)\,\mathrm{d}\tau, \tag{4.14}$$

$$E_V^* = \int_0^1 C_V(\tau)\dot{Y}(\tau)\,\mathrm{d}\tau. \tag{4.15}$$

In the simpler case where the displacement (Y), total force (C_Y) and vortex force (C_V) are sinusoidal functions given by

$$\left.\begin{aligned} Y &= A_Y^* \sin(2\pi\tau), \\ C_V &= C_{V0} \sin(2\pi\tau + \phi_V), \\ C_Y &= C_{Y0} \sin(2\pi\tau + \phi_Y), \end{aligned}\right\} \tag{4.16}$$

one can show that the energy transfer over a cycle (E^*) is given by

$$E^*/\pi A^* = [C_{Y0} \sin\phi_Y] = [C_{V0} \sin\,\phi_V]. \tag{4.17}$$

The idea of experimentally measuring a vortex force coefficient (C_{VO}), and a 'vortex phase' (ϕ_V), quite distinct from the classically used coefficient (C_Y) and phase (ϕ_Y) for the total force, was introduced in Govardhan & Williamson (2000). The vortex force, and the vortex phase in particular, are useful in that we relate the forces directly to the wake vortex motions and modes.

We now assemble profiles of the displacement $Y(\tau)$, the vortex force $C_V(\tau)$, and also the profile of the normalized energy transfer $\dot{e}_V(\tau)$, through a cycle. For simplicity, one can imagine, as for a child's swing, that when a body moves in a positive direction, then pushing in that positive direction, will input energy into the system. It is these concepts which lead to a key diagram in figure 16, but we briefly mention here the force, displacement and energy transfer plots in the later figures 17 and 18, which are aligned vertically to give a good physical understanding as to when, during a cycle, the force and velocity have the same sign, and therefore when the energy transfer is contributing positively to body motion. For each vortex mode and set of profiles, we include an image of the vorticity when there is a peak in energy transfer, and this corresponds to the small red symbol in the time traces.

If we now look ahead at figure 17(a) specifically, for the classical 2S mode, we see that maximum energy transfer occurs when the body is moving downwards, yielding ($\dot{Y} < 0$), and negative vortex force ($C_V < 0$), maximizing the product $\dot{e}_V$. We wish to understand what it is about the vortex dynamics, for each mode, that maximizes the energy transfer, and this will be particularly interesting in the case of the 2T mode discussed later. For the 2S mode, our maximum $\dot{e}_V$ appears to coincide with the shedding in the near wake of a strong clockwise blue vortex, so there is a dominance of clockwise vorticity translating downstream rapidly at this point, giving a large negative lift force C_V.

We shall now consider qualitatively the relationship between vorticity dynamics and force, in the manner adopted in Maull & Milliner (1978), Williamson (1985) and Obasaju, Bearman & Graham (1988). If we consider (4.1), it states that the vortex force on the body is equal to the rate of change of impulse of the vorticity distribution in the wake. In an approximate manner, we shall look at the lift force, F_V, due to the rate of change of impulse of the principal vortices in the near wake. (We assume approximately that other positive and negative vortices further downstream have effects which cancel out, and we note that F_V shown in the ensuing equations is lift force per unit cylinder length). We replace each distributed vortex qualitatively by a concentrated vortex of strength Γ, at vortex position $\{X_V, Y_V\}$ moving downstream relative to the body, at speed U_V (noting that U_V is the horizontal velocity of the vortex, minus the velocity of the image vorticity; see Graham 1980). The equivalent of equation (4.1) for a two-dimensional flow, suggests approximately, for a particular vortex of strength Γ, that

$$F_V = \rho \frac{\mathrm{d}}{\mathrm{d}t}(\Gamma X_V). \tag{4.18}$$

If we also consider here the dominant shedding vortex dynamics giving rise to the major peaks of lift vortex force, we write for a particular shedding vortex

$$F_V = \rho(\Gamma U_V). \tag{4.19}$$

In our example of Figure 17(a) for the straightforward 2S mode, when the dominant blue clockwise vortex is being shed, and is rapidly translating downstream, we find

$$\{U_V > 0; \Gamma < 0\} \Rightarrow F_V < 0;$$

therefore the lift force due to this blue vortex is acting downwards (negative) as seen in the force profile corresponding to the vorticity image (see the small red symbol within the time traces). In terms of non-dimensional parameters, we can introduce normalized vortex strength, $\Gamma^* = (\Gamma / UD)$, and normalized effective downstream

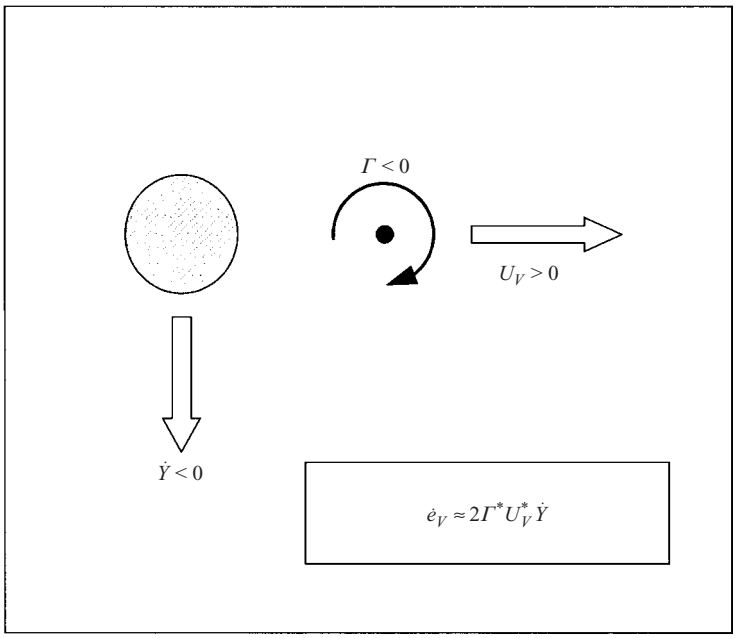

FIGURE 16. The key vortex motions contributing positive rate of energy transfer ($\dot{e}_V$) to the body motion due to the vorticity dynamics. There will be a peak energy transfer into vertical body vibration when there is a dominance of clockwise vorticity ($\Gamma < 0$) moving downstream to the right ($U_V > 0$), as the body moves downwards ($\dot{Y} < 0$). A similar situation would occur at the same point in the subsequent half cycle.

velocity, $U_V^* = (U_V/U)$, to give

$$\dot{e}_V = 2\Gamma^* U_V^* \dot{Y}. \tag{4.20}$$

In essence, we can say, in a qualitative manner:

There will be a peak energy transfer into vertical motion, when there is a dominance of clockwise vorticity moving downstream to the right, as the body moves downwards.

A diagram which illustrates this simple concept clearly is shown in figure 16. (We note that a similar peak energy transfer will be found in the following half-cycle, for the antisymmetric configuration.) Armed with these simple ideas, we can proceed to study the energy transfer for the other modes of figures 17 and 18.

For the 2P vortex mode of the lower branch of response, in figure 17(*b*), there is a peak in energy transfer, which again is when the body moves downwards during the translation of a dominant clockwise vortex downstream. We can write this mathematically as

$$\{\Gamma^* < 0; U_V^* > 0; \dot{Y} < 0\} \Rightarrow \dot{e}_V > 0.$$

In this case, it occurs at a distinctly different phase of the cycle than for the 2S mode, which is related to the fact that there is a switch in timing of vortex shedding for the 2P mode and the 2S mode (see Govardhan & Williamson 2000, figure 14). These examples are for small mass ratios, $m^* = 2.6$. However, the upper-branch 2P mode (see figure 18*a*), which we can only capture for larger mass ratios (here $m^* = 7.0$), also exhibits the same time history of energy transfer during a cycle as for the lower-branch 2P case.

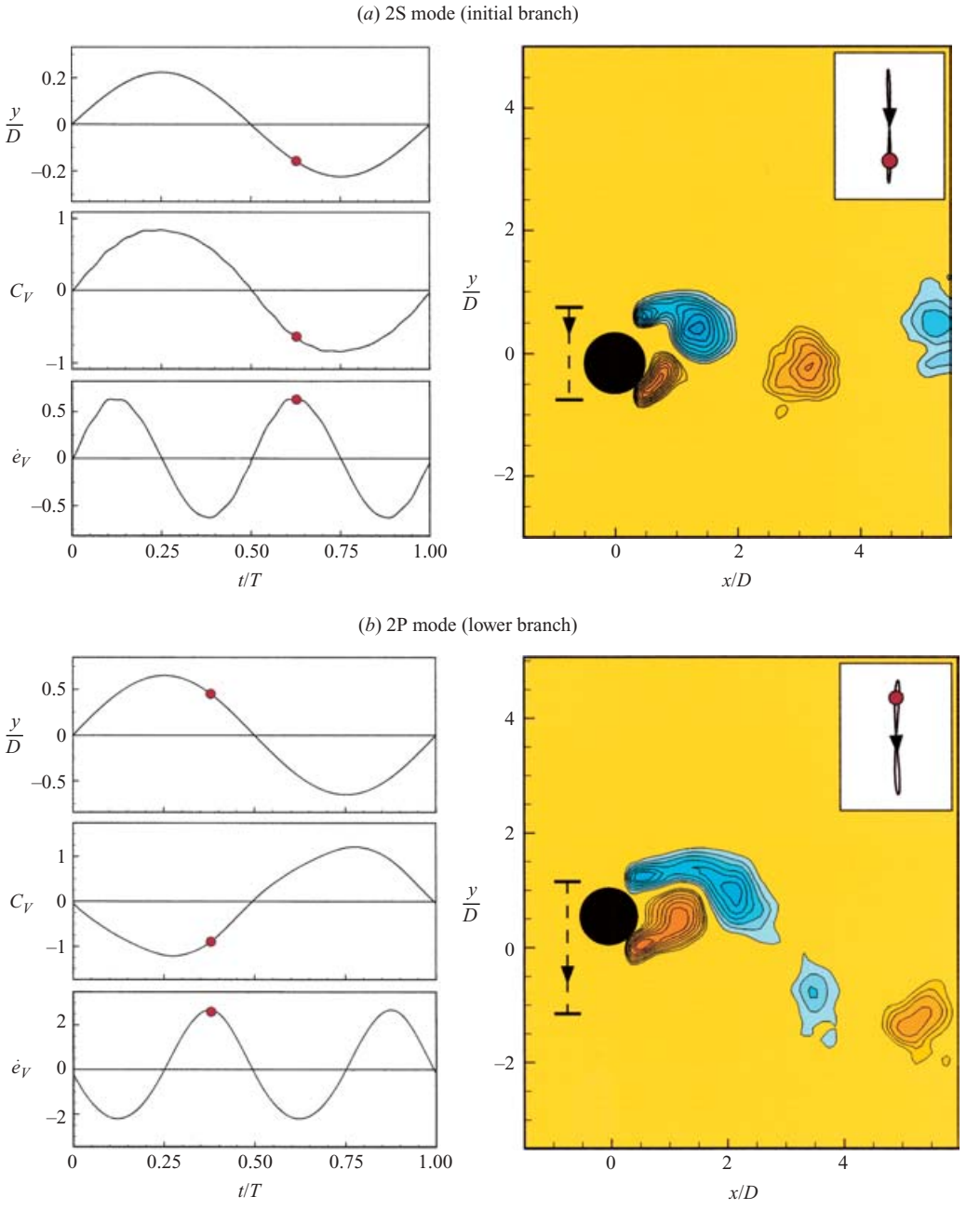

FIGURE 17. Rate of energy transfer due to vorticity dynamics ($\dot{e}_V$) for the 2S mode and for the lower-branch 2P mode, both for 'small' mass ratio ($m^* = 2.6$). Corresponding displacement $Y(t)$ and vortex force $C_V(t)$ profiles are shown. The vorticity images correspond to the red symbol in the time profiles on the left, at which points the rate of energy transfer due to vortex force ($\dot{e}_V$) is a maximum. The 2S mode is for $A^* = 0.25$; $U^* = 4.60$. The 2P mode is for $A^* = 0.65$; $U^* = 8.78$. Vorticity contour levels are $\{\omega D/U = \pm 0.5, \pm 1.0, \pm 1.5, \ldots\}$.

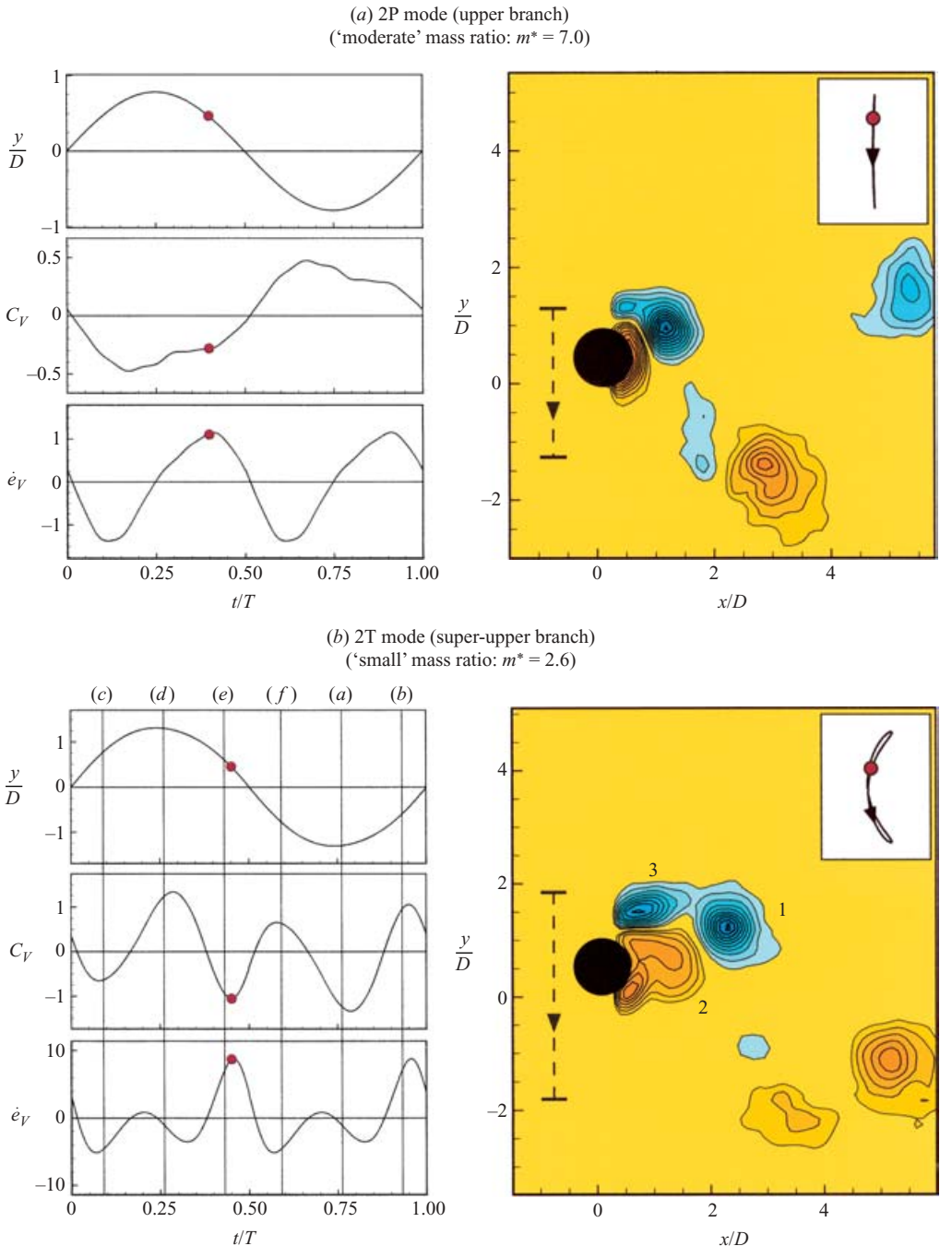

FIGURE 18. Rate of energy transfer due to vorticity dynamics ($\dot{e}_V$) for the upper-branch 2P mode ($m^* = 7.0$) and for the 2T mode ($m^* = 2.6$). Corresponding displacement $Y(t)$ and vortex force $C_V(t)$ profiles are shown. The vorticity images correspond to the red symbol in the time profiles on the left, at which points the rate of energy transfer due to vortex force ($\dot{e}_V$) is a maximum. The 2P mode is for $A^* = 0.78$; $U^* = 5.29$. The 2T mode is for $A^* = 1.33$; $U^* = 7.27$. Lines labelled (a) to (f) in (b) correspond to figure 11. Vorticity contours in (a) are $\{\omega D/U = \pm 0.5, \pm 1.0, \pm 1.5, \ldots\}$, and in ($b$) are $\{\omega D/U = \pm 0.4, \pm 1.2, \pm 2.0, \ldots\}$.

Finally, we can address the case of the 2T vortex formation mode, and ask which vortex motions are inducing such large vibrations? Which vortex motions contribute positive energy transfer into the body oscillations? Initially, we shall look again at the sequence of vorticity images in figure 11, and relate each image to its phase, each of which is marked as a thin vertical line in the force and displacement profiles of figure 18(*b*). Although the images do not correspond precisely to maximum and minimum of the energy transfer, it is serendipitous that in fact the images lie close to every maximum and minimum of the force profile $C_V(t)$. We have therefore marked, at the top right of each image in figure 11, the direction of lift force C_V (for example, positive force upwards is labelled C_V+). Let us start at the image (*e*); here we have the classical 2P vortex pair, namely vortex 1 and 2, but also an extra vortex 3. It is the combination and dominance of blue clockwise vorticity (vortex 1 and 3) translating downstream that can be associated with the negative peak of C_V, and in fact this is the phase during a cycle where the large peak of energy transfer into body motion appears, in figure 18. We can deduce that:

One can attribute the principal peak in energy transfer, as well as the emergence of this very high-amplitude response mode of the super-upper branch, to the formation and shedding of the third vortex of the 2T mode in each half-cycle.

Aside from the earlier approximate analysis of vortex dynamics, this statement appears consistent if one considers that without this third vortex, such large amplitudes are simply not attained. In order to complete an understanding of the sequence of force oscillations in figures 11 and 18, we now look at vorticity image (*f*), and it is the dominance of anticlockwise red vorticity moving downstream, in the near wake, that gives rise to a peak positive lift force:

$$\{U_V > 0; \Gamma > 0\} \Rightarrow F_V > 0.$$

The vigorous return of blue clockwise vorticity, generated on the body's downstroke, around the body clockwise at frame (*a*) causes the negative peak of C_V. Finally, the half-cycle is completed in (*b*), where we have the equivalent case to (*e*) discussed above, where the equivalent of vortices 1 and 3 cause a positive lift while the body moves upwards. At this point, we have again a strong peak of positive energy transfer into the body's motion from the fluid forces associated with vortex dynamics.

4.5. *In-line vortex modes*

In this section, we briefly show the vortex dynamics and X, Y trajectories for the in-line vibration modes, which appear for a frequency, $f_Y^* \sim 1/2$, and at the low normalized velocities of $U^* \sim 2.5$.

The streamwise antisymmetric (AS) mode exhibits an X, Y trajectory which takes the form of a figure-of-eight, with comparable streamwise and transverse amplitudes, as shown in figure 19(*b*). For each excursion of the body upstream, there is a vortex shed and left behind in the wake, and it is a feature of the antisymmetry of the mode that the trajectory is such a figure-of-eight, encouraging a different sign of vorticity to shed for each half-cycle. One might question whether the mode of vibration causes the antisymmetric vortex formation, or the pattern of formation causes the vibration, but it was found by Ongoren & Rockwell (1988) that this mode occurs with forced in-line

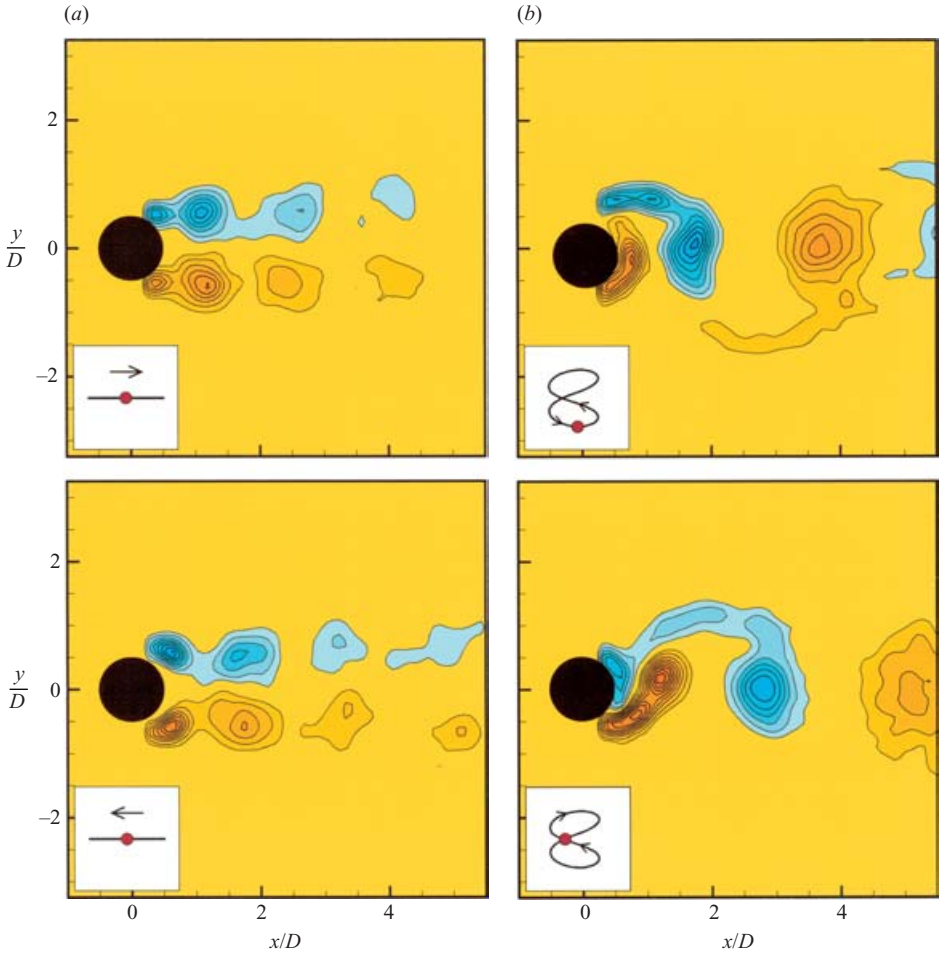

FIGURE 19. Streamwise vibration modes. (*a*) Streamwise symmetric mode (SS), where the motion is purely streamwise, forming a symmetric pair of vortices in each cycle. ($U^* = 2.14$; $A^*_X = 0.10$; $Re = 1600$). (*b*) Streamwise antisymmetric mode (AS), where the 2S vortex wake mode induces the body to move in a figure-of-eight X, Y trajectory. ($U^* = 3.03$; $A^*_X = 0.10$; $Re = 2200$). Vorticity contours are $\{\omega D/U = \pm 0.6, \pm 1.4, \pm 2.2, \ldots\}$.

(only) oscillations, so long as the frequency is below (and close to) the value $f^* = 0.5$. We conclude that the vortex formation induces the X, Y figure-of eight trajectory.

The second of these in-line vibration modes, defined as 'streamwise symmetric' (SS), represents a purely in-line motion, with symmetric pairs of wake vortices being generated in each cycle of in-line motion, as shown in figure 19(*a*). This corresponds with the 'first excitation' mode of a flexible cantilever, in the full-scale pile dynamics and laboratory experiments of Wooton *et al.* (1972), and King (1974). (Amplitudes for both modes ($A^*_X \sim 0.11$–0.13) compare reasonably with the cantilever responses ($A^*_X \sim 0.15$) measured by Wooton *et al.* (1972) and by King (1974); see also the book by Sumer & Fredsoe (1997)). It appears that when $U^* < 1/(2S)$, we have the streamwise symmetric mode, and when $U^* > 1/(2S)$, we have the streamwise antisymmetric mode. It is unclear why there exist two in-line modes, both able to impart positive energy to body motion.

5. Equations of motion and existence of a critical mass

In this section, we will present a pair of simple equations of motion to describe the dynamics of the body in both the X-direction and Y-direction (which is related to analogous equations derived earlier by F. Flemming; see Flemming & Williamson (2004). By using these equations, certain relationships between the X and Y motions will be deduced, and one of the key ingredients leading to these relationships is the fact that, for periodic vibrations, the streamwise oscillation frequency (f_X) is twice that for the transverse direction (f_Y):

$$f_X = 2f_Y. \tag{5.1}$$

We shall find, as discovered in the recent Y-only vibration studies in Govardhan & Williamson (2000, 2002), that there exists a critical mass (m^*_{crit}), below which the large-amplitude vibrations will persist, up to infinitely high normalized velocities, U^*. We evaluate the critical mass for the present X, Y dynamics, and find a reasonable agreement with the critical mass found from the Y-only studies above.

Two linear equations of motion, that represent our system in the X- and Y-directions are

$$m\ddot{y} + c\dot{y} + ky = F_Y(t), \tag{5.2a}$$
$$m\ddot{x} + c\dot{x} + kx = F_X(t). \tag{5.2b}$$

An excellent representation of the displacements in these experiments is

$$y(t) = A_Y \sin(\omega t), \tag{5.3a}$$
$$x(t) = A_X \sin(2\omega t + \theta), \tag{5.3b}$$

while a representation of the fluid forcing on the body, may be written

$$F_Y(t) = F_{Y0} \sin(\omega t + \phi_Y), \tag{5.4a}$$
$$F_X(t) = F_{X0} \sin(2\omega t + [\phi_X + \theta]). \tag{5.4b}$$

This representation of the fluid force fits the actual data less well as one approaches the top of the super-upper branch, but otherwise the use of such an equation can be shown to yield good results. (Even as one nears the top of the super-upper branch, one can take account of the non-sinusoidal nature of the fluid force, to yield excellent results even in that case. Such a study forms a part of the forthcoming papers by Williamson & Jauvtis (2004*a*, *b*)). A useful reference regarding the phases in equations (5.3)–(5.4), is given by the diagram of phase relationships in figure 1(*d*).

Straightforward solutions to equations (5.2)–(5.4), in the manner of Khalak & Williamson (1999), give the following set of equations. The forms of the equations are identical in the X- and Y-directions; one simply interchanges subscripts X for Y, except that for the frequencies one replaces f^*_Y by $2f^*_Y$, in accordance with equation (5.1).

$$f^*_X = 2f^*_Y, \tag{5.5}$$

$$A^*_Y = \frac{C_Y \sin\phi_Y}{4\pi^3(m^* + C_A)\zeta}\left(\frac{U^*}{f^*_Y}\right)^2 f^*_Y, \quad A^*_X = \frac{C_X \sin\phi_X}{4\pi^3(m^* + C_A)\zeta}\left(\frac{U^*}{2f^*_Y}\right)^2 2f^*_Y, \tag{5.6a,b}$$

$$f^*_Y = \sqrt{\frac{m^* + C_A}{m^* + C_{EAY}}}, \quad f^*_X = \sqrt{\frac{m^* + C_A}{m^* + C_{EAX}}}, \tag{5.7a,b}$$

$$C_{EAY} = \frac{C_Y \cos\phi_Y}{2\pi^3 A_Y^*}\left(\frac{U^*}{f_Y^*}\right)^2, \quad C_{EAX} = \frac{C_X \cos\phi_X}{2\pi^3 A_X^*}\left(\frac{U^*}{2f_Y^*}\right)^2; \tag{5.8a,b}$$

from A^* equations:

$$\left(\frac{A_X^*}{A_Y^*}\right) = \frac{1}{2}\left(\frac{C_X \sin\phi_X}{C_Y \sin\phi_Y}\right); \tag{5.9}$$

from f^* equations:

$$C_{EAX} = \tfrac{1}{4}C_{EAY} - \tfrac{3}{4}m^*. \tag{5.10}$$

The coefficient C_{EA} represents a force due to the vortex dynamics that is in phase with the body acceleration, and is not a true 'added mass', despite some recent discussion in the literature on this point. The coefficient C_A is the ideal added mass, and takes the value of 1.0. These equations have been discussed extensively for Y-only motion in the paper by Govardhan & Williamson (2000); in particular the equation for the frequency of the system formed the basis of much discussion:

$$f_Y^* = \sqrt{\frac{(m^* + C_A)}{(m^* + C_{EAY})}}, \tag{5.11}$$

and it was found, for an extensive set of experiments, that an excellent functional relationship between the frequency of the lower response branch f_{Ylower}^* and m^* could be deduced. (The frequency f_Y^* for the lower branch is quite constant, as typified by the branch marked L in figures 2 and 5.) The relationship was found to be accurately represented by the equation

$$f_{Ylower}^* = \sqrt{\frac{(m^* + 1)}{(m^* - 0.54)}}. \tag{5.12}$$

This equation led to the discovery of a critical mass, $m_{crit}^* = 0.54$, below which the lower branch ceases to exist. What happens is that the response amplitude of the upper branch persists to infinite normalized flow velocities, if $m^* < m_{crit}^*$ (as proven subsequently in Govardhan & Williamson 2002). One of the questions we have here for X, Y motion is: Does a critical mass exist also for this type of system?

It was shown in the later paper, Govardhan & Williamson (2002) that all vortex-induced vibration systems, which are represented well by equations such as (5.2)–(5.4), *will necessarily yield a critical mass.* Following this previous work, we now plot the frequency of the lower branch f_{Ylower}^*, for an extensive set of X, Y motion experiments conducted at different mass ratios, in figure 20. By fitting a least-squares best-fit curve, using the functional form of equation (5.11), we find, as shown in the figure:

$$f_{Ylower}^* = \sqrt{\frac{(m^* + C_A)}{(m^* - 0.52)}}. \tag{5.13}$$

This equation shows that for vortex-induced vibration of this X, Y system, the critical mass is evaluated as

$$m_{crit}^* = 0.52, \tag{5.14}$$

which is close to the value for Y-only motion. This similarity is to be expected since in the lower branch of response, the dynamics are primarily transverse, with little effect of streamwise vibration influencing the vortex formation mode or transverse response (see figure 2).

Finally, we should mention equations (5.9) and (5.10). Equation (5.9), which comes from a combination of the amplitude equations (5.6), relates the amplitudes to the

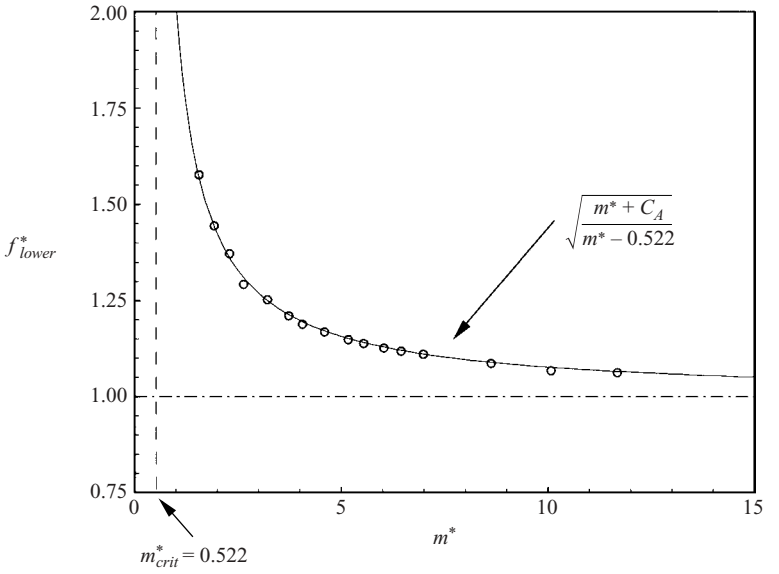

FIGURE 20. Evaluation of the 'critical mass' for X, Y motion, using extensive measurements of lower branch transverse frequency (f^*_{lower}) versus mass ratio (m^*). We evaluate the critical mass, $m^*_{crit} = 0.522$, from the least-squares best-fit of the frequency equation.

excitation in the X- and Y-directions, and we found that it fits the measured data reasonably. More useful though, is equation (5.10) which results from a combination of the frequency equations (5.7), which we recall is

$$C_{EAX} = \tfrac{1}{4} C_{EAY} - \tfrac{3}{4} m^*. \tag{5.15}$$

This is a simple equation which relates the effective added masses in the X- and Y-directions, and involves the mass ratio, m^*. It is particularly interesting because, if $m^* < m^*_{crit}$, then the frequency of the lower branch in equation (5.8) suggests that one will have a large response which persists to infinite U^*, but as explained in Govardhan & Williamson (2002), as the system tends to infinite U^* and infinite f^*

$$C_{EAY} = -m^*, \tag{5.16}$$

which gives the neat result, when combined with equation (5.10), that

$$C_{EAX} = C_{EAY}. \tag{5.17}$$

This is a significant result, because it ensures that, for a particular X, Y motion, if there is an infinite regime of resonance (an infinitely wide regime of large-amplitude vibration) for the Y dynamics, then this will also be the case for the X dynamics, and the shape of the X, Y trajectory will keep its form, as the normalized velocity extends to infinity. Of course, a simpler way to view this is to note that as U^* and f^*_Y extend to infinity, then f^*_X must also extend to infinity because of the fundamental frequency relationship in equation (5.1), namely $f^*_X = 2 f^*_Y$.

6. Concluding remarks

Despite the large number of papers dedicated to the problem of a cylinder vibrating transverse to a fluid flow (Y-motion), there are very few papers which allow the body

to vibrate in-line with the flow, as well as transverse to the free stream. Surprisingly, there are no experiments (to our knowledge) which address the most practical problem, namely a body in two degrees of freedom (X, Y-motion) where the oscillating mass is precisely the same in the transverse and in-line directions, and where the natural frequency is the same in both directions. For this purpose, we have designed the present pendulum apparatus to achieve both of these criteria. From these experiments, one of the principal questions which may be posed is:

How does the freedom to vibrate in-line with the flow influence the dynamics of the fluid and the structure?

Even down to the low mass ratios, where $m^* = 6$, it is remarkable that the freedom to oscillate in-line with the flow affects the transverse vibration surprisingly little. The same response branches, peak amplitudes, induced forces, and vortex wake modes are found for both Y-only and X, Y motion. If one increases the normalized velocities, one observes the initial branch (with a 2S vortex wake mode), the upper branch (with a 2P mode), and the lower branch (with a 2P mode), in close agreement with previous Y-only studies. It should also be mentioned that the response exhibits distinct response branches and wake modes, rather than the continuous response amplitude plots observed in the previous X, Y motion studies.

There is, however, a dramatic change in the fluid–structure interactions when mass ratios are reduced below $m^* = 6$. A new response branch with significant streamwise motion appears, in what we call the 'super-upper' branch, yielding massive amplitudes of 3 diameters peak-to-peak ($A_Y^* \sim 1.5$), which is far in excess of typical peak amplitudes for Y-only vibration ($A_Y^* \sim 1$). To present the response measurements, we introduce a three-dimensional plot where the Williamson–Roshko map of regimes (Y-only motion) forms the horizontal plane $\{(U^*/f^*)S$ versus $A_Y^*\}$, and where vertical height represents streamwise amplitude, A_X^*. The super-upper branch flies above the Williamson–Roshko map of regimes, but interestingly it both starts and terminates directly above the boundaries of the 2P mode for Y-only motion. Our super-upper branch is but one line within a possible continuous surface (or volume) of solutions for X, Y free vibration, which may exist in the space above the horizontal Williamson–Roshko regime map, and for which there would be positive energy transfer from fluid to body motion.

The discovery of a super-upper response branch corresponds to a new periodic vortex wake mode. This mode comprises a triplet of vortices being formed in each half-cycle, in what we define as a '2T' mode, following the terminology introduced in Williamson & Roshko (1988). The triplet strongly resembles the vortex pair formed in each half-cycle in the 2P mode, with the addition of a third strong vortex formed during the acceleration phase near the extremities of the transverse motion. A decomposition of the force into potential force and vortex force (following Lighthill 1986) yields the simple result that for any arbitrary periodic force and periodic displacement, the energy transfer from fluid to body motion over a cycle is given by the vortex force alone. We qualitatively interpret the vortex dynamics and vortex forces which yield a positive rate of energy transfer ($\dot{e}_V$) causing the body motion, using the following simple equation:

$$\dot{e}_V = 2\Gamma^* U_V^* \dot{Y}.$$

For example, this simple equation states that there is positive energy transfer into the body vibration when there is a dominance of clockwise vorticity ($\Gamma^* < 0$) moving

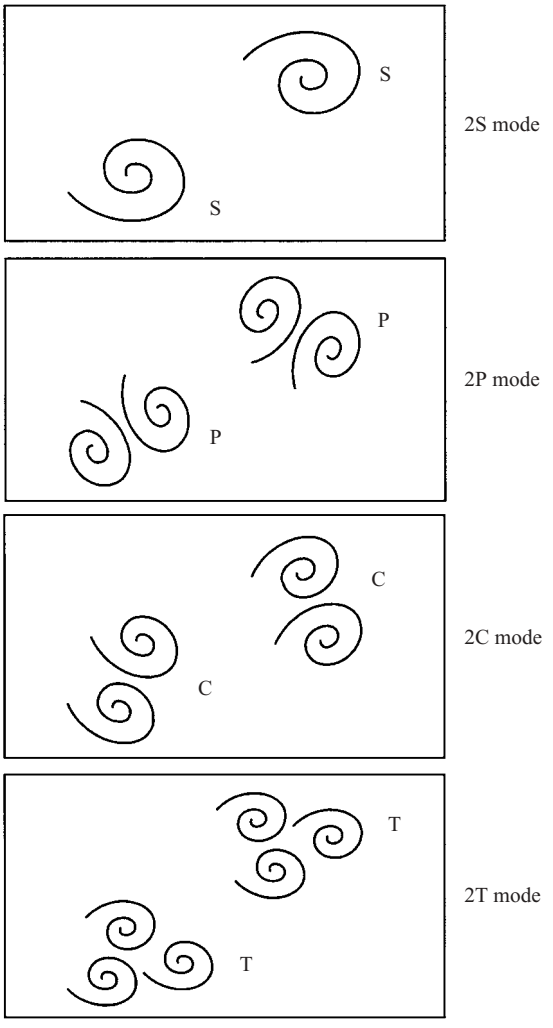

FIGURE 21. The set of vortex wake modes 2S, 2P, 2C, 2T which are known to contribute to vortex-induced vibration of cylindrical structures. All of these modes are antisymmetric. The 2C mode is found for the vibration of a pivoted cylinder (Flemming & Williamson, 2003). The 2T mode is found for X, Y motion. The 2S and 2P modes are observed in all these cases so far studied.

downstream to the right ($U_V^* > 0$), as the body moves downwards ($\dot{Y} < 0$). Using these qualitative ideas, it appears that the massive amplitudes of vibration for the 2T mode can be attributed to the energy transfer from the 'third' vortex of each triplet. This third vortex is not present in the case of the lower-amplitude 2P mode.

It appears that the 2T mode is the fourth vortex wake mode which contributes to vortex-induced vibration of such cylindrical structures. We summarize, in figure 21 (taken from Flemming & Williamson 2004), the set of four vortex wake modes:

$$\{2S, 2P, 2C, 2T\}$$

all of which have an antisymmetric symmetry. The 2C mode comprises a distinct pair of co-rotating vortices of the same sign generated in each half-cycle, and is found in

the pivoted cylinder experiments of Flemming & Williamson (2004). The 2T mode is found in the present X, Y motion experiments. The 2S and 2P modes are found in all cases including the transverse-only cylinder vibration. All of these vortex wake modes are generated by the body motion, while the vortices in turn provide positive energy transfer to continuously support the body motion.

We also find two in-line vibration modes for velocities below the regime of significant transverse vibration, when $U^* \sim 1/(2S) \sim 2.5$. When $U^* < 1/(2S)$, we find a streamwise symmetric vortex wake mode (SS). When $U^* > 1/(2S)$, we observe a streamwise antisymmetric vortex wake mode (AS). These two modes are not unexpected, and are equivalent to the first and second excitation modes of vibration for flexible cantilevers, discovered by Wooton *et al.* (1972) and King (1974).

By considering equations of motion for the two degrees of freedom, we find an equation for the frequency of motion, which involves both the mass ratio (m^*) and the effective added mass (C_{EA}). We deduce an expression for the transverse frequency of the lower branch of response, finding a constant value of $C_{EA} = 0.52$ which fits all of our experiments:

$$f^*_{Ylower} = \sqrt{\frac{(m^* + 1.0)}{(m^* - 0.52)}}.$$

This equation yields a critical mass, $m^*_{crit} = 0.52$, which is similar to the value (0.54) measured by Govardhan & Williamson (2000, 2002), below which the large-amplitude vibrations persist to infinite flow velocity. By further simple manipulation of the equations of motion, we find also

$$C_{EAX} = \tfrac{1}{4} C_{EAY} - \tfrac{3}{4} m^*,$$

relating the effective added mass in the transverse and streamwise directions. This neatly delivers the result $C_{EAX} = C_{EAY}$, when the mass is below critical, and when operating at large velocities. This is significant since it leads to the fact that the critical mass m^*_{crit} is the same for the X- and Y-directions, and ensures that the shapes (Lissajous figures) of X, Y trajectories can retain their form as the velocity becomes large.

In conclusion, we find that the freedom to move streamwise to the flow, as well as transverse, hardly changes the dynamics of elastically mounted cylinders, in the case of moderate mass ratios, $m^* > 6$. This indicates that the phenomena, and the extensive understanding, of vortex-induced vibration for Y-only body motions, built up over the last 35 years, remain of strong relevance to the case of two degrees of freedom. It is only for 'small' mass ratios, $m^* < 6$, that one observes a rather dramatic departure from previous results, yielding huge amplitudes of vibration, which would suggest a possible modification to the offshore design codes (for example Det Norske Veritas 2003) that have traditionally been based on results for bodies vibrating only transverse to the flow.

The authors thank very particularly Felix Flemming of TU Darmstadt, Germany, for immense help and camaraderie during the research itself, and the preparation of this manuscript. Danke Schoen, Felix! Thanks are due to others in the FDRL Team: Dr Raghu Govardhan of IISc., Bangalore, India; Matt Horowitz and Timothy Morse. The support from the Ocean Engineering Division of the ONR, monitored by Tom Swean, is gratefully acknowledged. (ONR Contract No. N00014-95-1-0332).

REFERENCES

Bearman, P. W. 1984 Vortex shedding from oscillating bluff bodies. *Annu. Rev. Fluid Mech.* **16**, 195–222.

Blackburn, H. M. & Karniadakis, G. E. 1993 Two- and three-dimensional simulations of vortex-induced vibration of a circular cylinder. In *Proc. 3rd Intl Offshore Polar Engng Conf. Singapore, 6–11 June 1993.*

Brika, D. & Laneville, A. 1993 Vortex-induced vibrations of a long flexible circular cylinder. *J. Fluid Mech.* **250**, 481–508.

Davis, J. T., Hover, F. S., Landolt, A. & Triantafyllou, M. S. 2000 Vortex-induced vibrations of rigid and flexible cylinders. In *Proc. WVIVOS – Workshop on Vortex-Induced Vibrations of Offshore Structures Sao Paulo, Brazil 14–16 August 2000* (ed. C. Pesce, J. Martins, J. Meneghini & J. Aranha), Paper #9. University of Sao Paulo.

Det Norske Veritas 2003 DNV Offshore Codes. *Det Norske Veritas* Hovik, Norway.

Feng, C. C. 1968 The measurement of vortex-induced effects in flow past stationary and oscillating circular and D-section cylinders. Master's thesis, University of British Columbia, Vancouver, BC, Canada.

Flemming, F. & Williamson, C. H. K. 2004 Vortex-induced vibrations of a pivoted cylinder. Submitted to *J. Fluid Mech.*

Govardhan, R. & Williamson, C. H. K. 1997 Vortex-induced motions of a tethered sphere. *J. Wind Engng Ind. Aerodyn.* **69–71**, 375–385.

Govardhan, R. & Williamson, C. H. K. 2000 Modes of vortex formation and frequency response of a freely vibrating cylinder. *J. Fluid Mech.* **420**, 85–130.

Govardhan, R. & Williamson, C. H. K. 2002 Resonance forever: existence of a critical mass and an infinite regime of resonance in vortex-induced vibration. *J. Fluid Mech.* **473**, 147–166.

Govardhan, R. & Williamson, C. H. K. 2004 Vortex-induced vibration of an elastically-mounted sphere. Submitted to *J. Fluid Mech.*

Graham, J. M. R. 1980 The forces on sharp-edged cylinders in oscillatory flow at low Keulegan-Carpenter numbers. *J. Fluid Mech.* **97**, 331–346.

Griffin, O. M. 1980 Vortex-excited cross-flow vibrations of a single cylindrical tube. *Trans. ASME: J. Pres. Vessel Tech.* **102**, 158–166.

Griffin, O. M. & Ramberg, S. E. 1976 Vortex shedding from a cylinder vibrating in line with an incident uniform flow. *J. Fluid Mech.* **75**, 257–271.

Griffin, O. M., Skop, R. A. & Ramberg, S. E. 1975 The resonant, vortex-excited vibrations of structures and cable systems. In *7th Ann. Offshore Technology Conf. Houston, TX, USA*, OTC Paper 2319.

Hover, F. S., Davis, J. T. & Triantafyllou, M. S. 2004 Three-dimensionality of mode transition in vortex-induced vibrations of a circular cylinder. *Eur. J. Mech.* B-*Fluids* **23**, 29–40.

Jauvtis, N. & Williamson, C. H. K. 2002*a* Vortex-induced vibration, of a cylinder in two degrees of freedom. In *Proc. BBVIV-3 Bluff Body Wakes and Vortex-Induced Vibrations, Port Douglas, Australia, 17–20 December 2002* (ed. K. Hourigan, T. Leweke, M. C. Thompson & C. H. K. Williamson), pp. 53–56. Monash University, Melbourne.

Jauvtis, N. & Williamson, C. H. K. 2002*b* X-Y Vortex-induced vibration of a cylinder. *Bull. Am. Phys. Soc.* **47**, 145.

Jauvtis, N. & Williamson, C. H. K. 2003 Vortex-induced vibration of a cylinder with two degrees of freedom. *J. Fluids Struct.* **17**, 1035–1042.

Jeon, D. & Gharib, M. 2001 On circular cylinders undergoing two-degree-of-freedom forced motions. *J. Fluids Struct.* **15**, 533–541.

Khalak, A. & Williamson, C. H. K. 1996 Dynamics of a hydroelastic cylinder with very low mass and damping. *J. Fluids Struct.* **10**, 455–472.

Khalak, A. & Williamson, C. H. K. 1997 Fluid forces and dynamics of a hydroelastic structure with very low mass and damping. *J. Fluids Struct.* **11**, 973–982.

Khalak, A. & Williamson, C. H. K. 1999 Motions, forces and mode transitions in vortex-induced vibrations at low mass-damping. *J. Fluids Struct.* **13**, 813–851.

King, R. 1974 Vortex excited structural oscillations of a circular cylinder in steady currents. In *6th Ann. Offshore Technology Conf. Houston, TX, USA*, OTC Paper 1948.

Lighthill, J. 1986 Wave loading on offshore structures. *J. Fluid Mech.* **173**, 667–681.

Maull, D. J. & Milliner, M. C. 1978 Sinusoidal flow past a circular cylinder. *Coastal Engng* **2**, 149–168.

Moe, G. & Wu, Z.-J. 1990 The lift force on a cylinder vibrating in a current. *Trans. ASME: J. Offshore Mech. Arctic Engng* **112**, 297–303.

Naudascher, E. 1987 Flow-induced streamwise vibrations of structures. *J. Fluids Struct*. **1**, 265–298.

Newman, D. & Karniadakis, G. E. 1995 Direct numerical simulations of flow over a flexible cable. In *Flow-Induced Vibration* (ed. P. W. Bearman). Balkema, Rotterdam.

Newman, D. & Karniadakis, G. E. 1996 Simulations of flow over flexible cable: a comparison of forced and flow-induced vibration. *J. Fluids Struct*. **10**, 439–453.

Obasaju, E. D., Bearman, P. W. & Graham, J. M. R. 1988 A study of forces, circulation and vortex patterns around a circular cylinder in oscillating flow. *J. Fluid Mech*. **196**, 467–494.

Okajima, A., Nakamura, A., Kosugi, T. & Uchida, H. 2002 Flow-induced in-line oscillations of a circular cylinder. In *Proc. BBVIV-3 Bluff Body Wakes and Vortex-Induced Vibrations Port Douglas, Australia, 17–20 December 2002* (ed. K. Hourigan, T. Leweke, M. C. Thompson & C. H. K. Williamson). Monash University, Melbourne.

Ongoren, A. & Rockwell, D. 1988 Flow structure from an oscillating cylinder. Part 2. Mode competition in the near wake. *J. Fluid Mech*. **191**, 225–245.

Sarpkaya, T. 1979 Vortex-induced oscillations. *Trans. ASME J. Appl. Mech*. **46**, 241–258.

Sarpkaya, T. 1995 Hydrodynamic damping, flow-induced oscillations, and biharmonic response. *Trans. ASME: J. Offshore Mech. Arctic Engng* **117**, 232–238.

Sugimoto, T., Saito, S., Matsuda, K., Okajima, A., Kiwata, T. & Kosugi, T. 2002 Water tunnel experiments on in-line oscillations of a circular cylinder with a finite span length. In *Proc. BBVIV-3 Bluff Body Wakes and Vortex-Induced Vibrations Port Douglas, Australia, 17–20 December 2002* (ed. K. Hourigan, T. Leweke, M. C. Thompson & C. H. K. Williamson). Monash University, Melbourne.

Sumer, B. M. & Fredsoe, J. 1997 *Hydrodynamics around Cylindrical Structures*. World Scientific.

Williamson, C. H. K. 1985 Sinusoidal flow relative to circular cylinders. *J. Fluid Mech*. **155**, 141–174.

Williamson, C. H. K. & Govardhan, R. 2004 Vortex-induced vibrations. *Annu. Rev. Fluid Mech*. **36**, 413–455.

Williamson, C. H. K. & Jauvtis, N. 2004*a* The effects of non-harmonic forcing in vortex-induced vibration. In preparation for *J. Fluid Mech*.

Williamson, C. H. K. & Jauvtis, N. 2004*b* A high-amplitude 2 T mode of vortex formation, and the effects of non-harmonic forcing in vortex-induced vibration. To appear in *Eur. J. Mech*. B-*Fluids*.

Williamson, C. H. K. & Roshko, A. 1988 Vortex formation in the wake of an oscillating cylinder. *J. Fluids Struct*. **2**, 355–381.

Wooton, L. R., Warner, M. H., Sainsbury, R. N. & Cooper, D. H. 1972 Oscillations of piles in marine structures. A resume of full-scale experiments at Immingham. *CIRIA Tech. Rep*. 41.